

†Deceased 28 January 2021.

**Special Section:**

The Curiosity rover's investigation of Glen Torridon and the surrounding area

**Key Points:**

- Sample Analysis at Mars data indicated Fe-smectite, carbonate, oxidized organics, Fe/Mg sulfates, and chlorides in Glen Torridon (GT) rocks
- GT's environmental history involved fluids of variable redox potential and chemistry under a range of fluid-to-rock ratios
- Fluid episodes could have provided habitable environments and carbon was present, but nitrogen could have been a limiting factor

**Supporting Information:**

Supporting Information may be found in the online version of this article.

**Correspondence to:**

A. C. McAdam,  
[Amy.McAdam@nasa.gov](mailto:Amy.McAdam@nasa.gov)

**Citation:**

McAdam, A. C., Sutter, B., Archer, P. D., Franz, H. B., Wong, G. M., Lewis, J. M. T., et al. (2022). Evolved gas analyses of sedimentary rocks from the Glen Torridon clay-bearing unit, Gale crater, Mars: Results from the Mars Science Laboratory Sample Analysis at Mars instrument suite. *Journal of Geophysical Research: Planets*, 127, e2022JE007179. <https://doi.org/10.1029/2022JE007179>













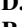




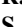









Received 24 JAN 2022

Accepted 3 JUN 2022

© 2022 The Authors. This article has been contributed to by U.S. Government employees and their work is in the public domain in the USA.

This is an open access article under the terms of the [Creative Commons Attribution-NonCommercial-NoDerivs License](https://creativecommons.org/licenses/by/4.0/), which permits use and distribution in any medium, provided the original work is properly cited, the use is non-commercial and no modifications or adaptations are made.

## Evolved Gas Analyses of Sedimentary Rocks From the Glen Torridon Clay-Bearing Unit, Gale Crater, Mars: Results From the Mars Science Laboratory Sample Analysis at Mars Instrument Suite

A. C. McAdam<sup>1</sup> , B. Sutter<sup>2,3</sup> , P. D. Archer<sup>2,3</sup> , H. B. Franz<sup>1</sup> , G. M. Wong<sup>4</sup> , J. M. T. Lewis<sup>1,5,6</sup> , J. V. Clark<sup>2,7</sup> , M. Millan<sup>1,8</sup> , A. J. Williams<sup>9</sup> , J. L. Eigenbrode<sup>1</sup> , C. A. Knudson<sup>1,10</sup> , C. Freissinet<sup>11</sup> , D. P. Glavin<sup>1</sup> , J. C. Stern<sup>1</sup> , R. Navarro-González<sup>12,†</sup> , C. N. Achilles<sup>1,10</sup> , D. W. Ming<sup>2</sup> , R. V. Morris<sup>2</sup> , T. F. Bristow<sup>13</sup> , E. B. Rampe<sup>2</sup> , M. T. Thorpe<sup>14</sup> , C. H. House<sup>4</sup> , S. Andrejkovičová<sup>15</sup> , A. B. Bryk<sup>16</sup> , V. K. Fox<sup>17</sup> , S. S. Johnson<sup>8</sup> , P. R. Mahaffy<sup>1</sup> , and C. A. Malespin<sup>1</sup>

<sup>1</sup>NASA Goddard Space Flight Center, Greenbelt, MD, USA, <sup>2</sup>NASA Johnson Space Center, Houston, TX, USA, <sup>3</sup>Jacobs Technology, Houston, TX, USA, <sup>4</sup>Department of Geosciences, The Pennsylvania State University, University Park, PA, USA, <sup>5</sup>Department of Physics and Astronomy, Howard University, Washington, DC, USA, <sup>6</sup>Center for Research and Exploration in Space Science and Technology, NASA GSFC, Greenbelt, MD, USA, <sup>7</sup>GeoControls Systems – JETS Contract at NASA Johnson Space Center, Houston, TX, USA, <sup>8</sup>Department of Biology, Georgetown University, Washington, DC, USA, <sup>9</sup>Department of Geological Sciences, University of Florida, Gainesville, FL, USA, <sup>10</sup>Center for Research and Exploration in Space Science and Technology, University of Maryland, College Park, MD, USA, <sup>11</sup>Laboratoire Atmosphère, Milieux, Observations Spatiales (LATMOS), LATMOS/IPSL, UVSQ Université Paris-Saclay, Sorbonne Université, CNRS, Guyancourt, France, <sup>12</sup>Instituto de Ciencias Nucleares, Universidad Nacional Autónoma de México, Ciudad Universitaria, México City, Mexico, <sup>13</sup>NASA Ames Research Center, Moffett Field, CA, USA, <sup>14</sup>Texas State University, JETS, at NASA Johnson Space Center, Houston, TX, USA, <sup>15</sup>Geosciences Department, Geobiotec Unit, Aveiro University, Aveiro, Portugal, <sup>16</sup>Department of Earth and Planetary Science, University of California Berkeley, Berkeley, CA, USA, <sup>17</sup>Department of Earth and Environmental Sciences, University of Minnesota, Minneapolis, MN, USA

**Abstract** Evolved gas analysis (EGA) data from the Sample Analysis at Mars (SAM) instrument suite indicated Fe-rich smectite, carbonate, oxidized organics, Fe/Mg sulfate, and chloride in sedimentary rocks from the Glen Torridon (GT) region of Gale crater that displayed phyllosilicate spectral signatures from orbit. SAM evolved H<sub>2</sub>O data indicated that the primary phyllosilicate in all GT samples was an Fe-rich dioctahedral smectite (e.g., nontronite) with lesser amounts of a phyllosilicate such as mixed layer talc-serpentine or greenalite-minnesotaite. CO<sub>2</sub> data supported the identification of siderite in several samples, and CO<sub>2</sub> and CO data was also consistent with trace oxidized organic compounds such as oxalate salts. SO<sub>2</sub> data indicated trace and/or amorphous Fe sulfates in all samples and one sample may contain Fe sulfides. SO<sub>2</sub> data points to significant Mg sulfates in two samples, and lesser amounts in several other samples. A lack of evolved O<sub>2</sub> indicated the absence of oxychlorine salts and Mn<sup>3+</sup>/Mn<sup>4+</sup> oxides. The lack of, or very minor, evolved NO revealed absent or very trace nitrate/nitrite salts. HCl data suggested chloride salts in GT samples. Constraints from EGA data on mineralogy and chemistry indicated that the environmental history of GT involved alteration with fluids of variable redox potential, chemistry and pH under a range of fluid-to-rock ratio conditions. Several of the fluid episodes could have provided habitable environmental conditions and carbon would have been available to any past microbes though the lack of significant N could have been a limiting factor for microbial habitability in the GT region.

**Plain Language Summary** The Mars Science Laboratory Curiosity rover carried out a comprehensive investigation of the sedimentary rocks in the Glen Torridon (GT) region in Gale crater, Mars, to better understand Martian geologic history. The rover's Sample Analysis at Mars instrument suite was used to heat samples from GT and detect gases that were evolved to help identify the volatile-bearing mineralogy of the samples. Results indicated the presence of Fe-rich smectite, carbonate, oxidized organics, Fe and Mg sulfate, and chloride while oxychlorine salts, Mn<sup>3+</sup>/Mn<sup>4+</sup> oxides, and nitrate/nitrite salts were either not detected or occurred in trace amounts. This mineralogy data implied that geochemical conditions and fluid-to-rock ratios varied over time and that the conditions of GT depositional and diagenetic environments would have been amenable to microbial life with sufficient carbon but nitrogen abundances could have been limiting.

## 1. Introduction

The Mars Science Laboratory (MSL) Curiosity rover has been exploring Aeolis Mons, informally known as Mount Sharp, in Gale crater to understand the geological and environmental history and potential habitability recorded in the mineralogy and chemistry of its strata (Grotzinger et al., 2012). Orbital observations of the strata indicated mineralogical variations, including different abundances of sulfates, phyllosilicates, and hematite (e.g., Fraeman et al., 2013, 2016; Milliken et al., 2010). These observations identified a phyllosilicate-rich region and investigation of this layer has been a much-anticipated goal for Curiosity. Phyllosilicates can be key indicators of habitable environments, the detailed characteristics of those phyllosilicates can constrain the nature of the habitable environments (e.g., pH, open vs. closed system alteration), and these minerals can possibly facilitate the preservation of organic compounds (e.g., Bristow et al., 2015; Farmer & Des Marais, 1999; Grotzinger et al., 2014; Millan et al., 2020; Wattel-Koekkoek et al., 2003; Williams et al., 2019). In addition, sulfate-bearing layers overlie the phyllosilicate-rich layer and this sequence may record a large-scale environmental change over time (Milliken et al., 2010) so the environmental history gleaned from study of the phyllosilicate-rich layer can inform conditions at the beginning of this significant transition. Finally, assessment of how environments recorded in the phyllosilicate-rich layer fit into the story recorded in the underlying fluvio-lacustrine sedimentary rocks, and the nearby diagenetically altered hematite-bearing layer exposed in Vera Rubin ridge (VRR), will enable further insights into Gale crater's geological history. Curiosity investigated this phyllosilicate-rich layered region, or clay-bearing unit, termed "Glen Torridon" (GT) (Figure 1), with its suite of instruments between sols (Martian day) 2,300 and 3,050.



**Figure 1.** Glen Torridon region explored by Curiosity (Calef & Parker, 2016) with rover traverse indicated in yellow and drill sites marked with green circles and labeled in green. White dotted lines mark boundaries between members. After Figure 5 in Bennett et al., 2022. Drill sites and members are described further below.

## 2. Overview of Glen Torridon Geology

The stratigraphically lowest GT rocks, of the Jura member (Jm), had textures and bulk chemistry indicating that they are likely a continuation of the Murray formation (Mf) (e.g., Fox et al., 2020; O’Connell-Cooper et al., 2022). The Murray formation in Mt. Sharp is a stack of fluvial-lacustrine deposits >300 m thick (Fedo et al., 2018) that Curiosity has been exploring since 2,014. The Jura member in GT was primarily a fine-grained mudstone and was observed to consist of two different morphologies, a “rubbly Jura” expressed as dominantly rubble with rare bedrock patches and a “coherent Jura.” Rubbly Jura was mainly comprised of finely laminated mudstones while coherent Jura was coarser grained (e.g., Dehouck et al., 2022). These rocks are stratigraphically equivalent to the Jura member rocks studied by Curiosity on VRR (Fedo et al., 2020).

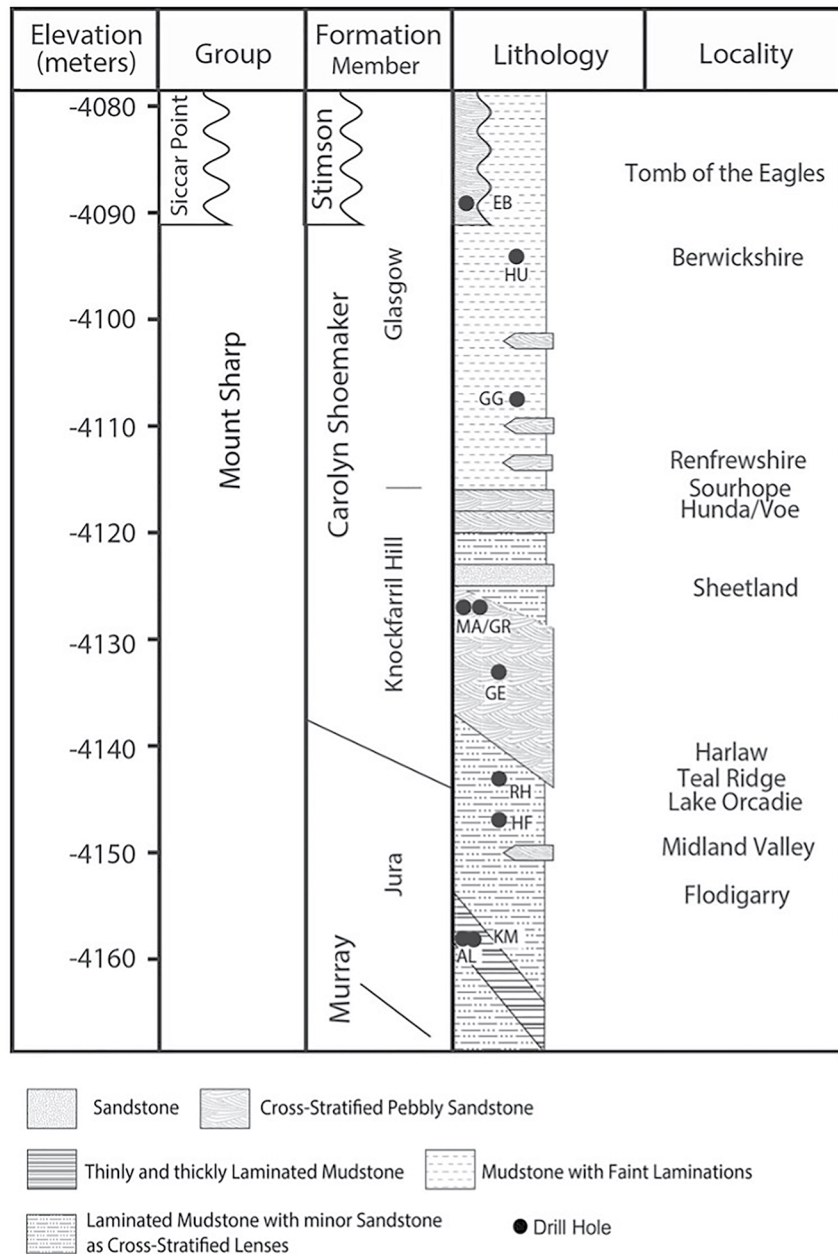


**Figure 2.** Stratigraphic column showing context of drill samples acquired during the Glen Torridon (GT) campaign, and two drill samples from Vera Rubin ridge (VRR), that are discussed in this manuscript. The GT samples are KM (Kilmarie), Glen Etive (GE), Mary Anning (MA), Groken (GR), and Glasgow (GG). The VRR samples are Highfield (HF) and Rockhall (RH). Column credit: The Mars Science Laboratory Sed-Strat Working Group.

Above the Jura member, Curiosity observed a change in lithology that warranted the naming of a new formation, the Carolyn Shoemaker formation (CSf), which was subdivided into the Knockfarril Hill member (KHm) and the Glasgow member (Gm) (Figure 2). The KHm consisted of mainly cross-bedded sandstones (Fedo et al., 2022; Fox et al., 2020). The Gm consisted of faintly laminated mudstone (Fedo et al., 2022). A variety of diagenetic features were observed in GT including nodules and vein fills (Gasda et al., 2022). Gm exhibited a significant number of diagenetic features which were less common in the underlying KHm (e.g., Gasda et al., 2022; O'Connell-Cooper et al., 2022). As seen throughout Gale crater, Ca sulfate filled veins were also observed in GT rocks (Gasda et al., 2022).

The mineralogy derived from Chemistry and Mineralogy (CheMin) instrument X-ray diffraction (XRD) analyses revealed several key observations of GT sample clay, sulfate and iron oxide mineralogy, as well as additional characteristics important for constraining the geologic history recorded in materials of GT, the adjacent VRR, and the stratigraphically lower Murray formation. The primary minerals plagioclase feldspar, pyroxene, and potassium feldspar (in small abundances) were detected in all samples but Jm member samples showed lower feldspar abundances compared to other GT samples (Thorpe et al., 2022). All samples also contained small amounts of hematite, in contrast to samples from the nearby VRR that were relatively enriched in hematite, and a range of Ca sulfate abundances with the Jura sample KM being most enriched in Ca sulfate minerals (~11 wt. %) and Knockfarril Hill sample GR being the least enriched (~4.3 wt. %) (Thorpe et al., 2022). The Jura KM sample, and the KHm MA, GR and GE samples display XRD evidence of the Fe carbonate siderite, the first high likelihood detection of carbonate by CheMin, in abundances ranging from ~0.8 to ~3.2 wt. % (Thorpe et al., 2022).

High clay mineral abundances were detected in all GT samples including the highest detected by CheMin to date (~34 wt. %, in the GE sample) (Bristow et al., 2021; Thorpe et al., 2022). The detected clay minerals consist mainly of Fe-rich dioctahedral smectite (Thorpe et al., 2022). In the Jura member KM sample, and Knockfarril Hill member GR and MA samples, CheMin also made the first detection of a phase giving a sharp XRD pattern peak at 9.2 Å consistent with minnesotaite interstratified with minor greenalite (G-M) (Thorpe et al., 2022) or Fe talc interstratified with minor serpentine (S-T) (Bristow et al., 2021). The area in the KHm where the GR and MA samples were collected exhibited dark-toned Mn-rich nodules and Mn-rich bedrock, and ChemCam instrument observations of a large fraction of the nodules also showed elevated phosphorous (Gasda et al., 2022). Despite these increased concentrations of Mn and P, CheMin data were not interpreted to indicate a crystalline Mn, P bearing phase (Bristow et al., 2021; Thorpe et al., 2022). Finally, X-ray amorphous materials were observed in all GT samples with abundances ranging from ~25 to 47 wt. % (Thorpe et al., 2022). Determining the nature of the amorphous material is challenging; it can consist of glasses, a variety of alteration products including nanophase Fe-oxides and sulfate salts, or a combination of these (e.g., Bish et al., 2013; Thorpe et al., 2022).

### 3. SAM Background

The Sample Analysis at Mars (SAM) instrument suite (Mahaffy et al., 2012) has informed the nature of volatile-bearing phases in materials sampled by Curiosity. SAM evolved gas analysis (EGA) mass spectrometry measurements, during which samples are heated and any volatiles evolved are detected by a mass spectrometer, have found H<sub>2</sub>O, CO<sub>2</sub>, O<sub>2</sub>, H<sub>2</sub>, SO<sub>2</sub>, H<sub>2</sub>S, HCl, NO, CO, and other volatiles, including organic fragments (e.g., Leshin et al., 2013; McAdam et al., 2020; Ming et al., 2014; Sutter et al., 2017). The temperature of evolution and identity of evolved gases can support mineral detection by CheMin XRD analyses, indicate the presence of trace volatile-bearing phases present at abundances below CheMin detection limits, and constrain the nature of materials difficult to identify with XRD (e.g., X-ray amorphous materials). For example, temperatures of H<sub>2</sub>O evolution during Sample Analysis at Mars evolved gas analysis (SAM EGA) analyses have informed the likely octahedral chemistry and occupancy of phyllosilicates observed by CheMin (Bristow et al., 2018; McAdam et al., 2017; Sutter et al., 2017). In addition, SAM EGA analyses have indicated the presence of several different types of either X-ray amorphous or trace Mg sulfates, Fe sulfates/sulfides, oxychlorine salts, and/or nitrate/nitrite salts in many samples analyzed by MSL (e.g., Glavin et al., 2013; Stern et al., 2015; Sutter et al., 2017). SAM analyses of GT samples have also enabled constraints on sample phyllosilicate and salt mineralogy, which are reported in this work.

In addition to constraints on mineralogy, SAM has also enabled studies of the organic chemistry of analyzed samples, and possible associations between organic compounds and minerals, two primary goals of the SAM instrument suite. For example, SAM analyses have revealed chlorohydrocarbons (Freissinet et al., 2015) and sulfur-bearing organic compounds (Eigenbrode et al., 2018) in some Gale crater samples. Similarity, in some samples, in the temperatures of evolution of sulfur-bearing organics and SO<sub>2</sub> evolutions from sulfate thermal decomposition suggests that there may be a relationship between the organics and sulfur minerals (Eigenbrode et al., 2018; Francois et al., 2016; Lewis et al., 2019). Several GT samples have also shown evidence of organic compounds in SAM analyses. During Curiosity's GT campaign, SAM analyzed several samples with its pyrolysis gas chromatography mass spectrometry (GCMS) and wet chemistry experiments (derivatization with MTBSTFA [*N*-methyl-*N*-(*tert*-butyldimethylsilyl) trifluoroacetamide] in its solvent dimethylformamide, 4:1 by volume, and thermochemolysis with TMAH (25 wt. % tetramethylammonium hydroxide in methanol). These analyses indicated a diversity of organic compounds (Millan et al., 2022; Williams et al., 2021). While some of the organic molecules detected are related to SAM's wet chemistry experiment reagents and related background, it is also likely that some sulfur-containing organics evolved from samples at high pyrolysis temperatures are indigenous to the sample. Though the origin (meteoritic infall, geological sources, biological sources) is difficult to determine with the available data, the SAM data have helped address Curiosity's goal to determine if organics are preserved in the GT clay-bearing unit (Millan et al., 2022).

Here we present an overview of the SAM EGA results from GT samples, the constraints on sample mineralogy and geochemistry enabled by these results and, in the context of other rover analyses, the implications of these results for the depositional and alteration conditions experienced by GT materials.

## 4. Methods

### 4.1. SAM Instrument Suite Analyses

The SAM instrument suite is composed of a quadrupole mass spectrometer (QMS), a six-column gas chromatograph (GC) and a tunable laser spectrometer (TLS) coupled by solid and gas sample processing systems including two pyrolysis ovens (Mahaffy et al., 2012). These instruments were used to measure the abundances and isotopic composition of volatiles released during heating of samples, as well as martian atmosphere, but here we focus on volatiles evolved during pyrolysis. In SAM's EGA mode, samples were heated and any volatiles evolved were measured directly by the QMS. SAM's GCMS mode was used to analyze organic and inorganic gases evolved during sample heating. SAM's TLS mode was used to measure the amounts and isotopic composition of H<sub>2</sub>O, CO<sub>2</sub>, and CH<sub>4</sub> gases evolved during pyrolysis. For TLS or GC analyses during a given run, the volatiles released from the sample over a chosen temperature range (termed a "cut") were sent to those instruments to be measured. A TLS cut or a GC cut can be obtained during a given SAM sample heating run, and in either type of run, direct monitoring of the evolved volatiles to give EGA data was also carried out. Both the pyrolysis-TLS and pyrolysis-GCMS modes were used during SAM analyses of GT samples, as well as two types of wet chemistry experiments (Millan et al., 2022; Williams et al., 2021).

Here we focus on major volatile data from SAM's EGA mode. EGA analysis results in signal versus temperature curves referred to as EGA traces. During EGA analysis, a subsample of a given drill sample was delivered to a sample cup in SAM's Sample Manipulation System (SMS). For several GT drill samples, SAM carried out both pyrolysis-TLS and pyrolysis-GCMS analyses (and in some cases also wet chemistry analyses). This is facilitated by drill samples large enough to provide several subsamples to SAM (and also CheMin). However, beyond a certain number of needed subsamples a second drill hole must be acquired and this approach was used twice in GT. Since EGA data is obtained during every pyrolysis-TLS run and every pyrolysis-GCMS run of a subsample, EGA data was acquired from several subsamples of a given drill sample in some cases. In these cases, the EGA runs were numbered and some GT samples had as many as three EGA runs on three different subsamples. Before receiving a sample, sample cups were preconditioned by heating the cup in one of SAM's ovens to ~900°C for 5 min in order to mitigate signals from SAM's background during sample analysis. The preconditioned cups were removed from the oven to receive sample and then placed back into the oven and heated from ~40°C to ~900°C at an average temperature ramp rate of 35°C/min. Gas manifold lines within SAM are maintained at 135°C during runs to facilitate flow of evolved gases through the manifold. Volatiles released from samples were carried by an

He carrier gas (~0.8 standard cubic centimeters per minute, ~25 mb) to the QMS where they were detected by the mass-to-charge ratio ( $m/z$ ) of the molecule, one of its isotopologues, or one of its MS fragments.

#### 4.2. EGA Data Processing

Most EGA analyses of GT samples were carried out in SAM's Oven #1, but some were carried out using SAM's Oven #2. The ovens are similar except that Oven #1 has a temperature sense wire and Oven #2 instead has a second heater wire; this difference results in Oven #2 having the capability to reach slightly higher temperatures (Mahaffy et al., 2012). The approach for determination of sample temperature for Oven #1 has not changed throughout the course of the mission, but the preferred approach for modeling Oven #2 sample temperature was updated by the science team several years ago. The sample temperature model used for the Oven #2 EGA plots and interpretations discussed here was the "oven-2\_model-1" model (Franz et al., 2020).

For some EGA runs, the QMS signal for the main  $m/z$  of a molecule was saturated. In these cases, the unsaturated signal or the isotopologue or ionization fragment (formed by fragmentation in the detector) was plotted to represent the molecule (these signals will track with temperature the same as the main molecule  $m/z$  so they can be used to depict trends in the main molecule when the main  $m/z$  signal is saturated) (e.g., Archer et al., 2014). For example, the signal at the main  $m/z$  of  $H_2O$  ( $m/z$  18) was saturated in EGA analyses so  $m/z$  17 (OH fragment of  $H_2O$ ) or  $m/z$  20 ( $m/z$  dominated by the  $H_2^{18}O$  isotopologue of  $H_2O$ ) was plotted to depict the  $H_2O$  signal versus temperature.

The interpretation of EGA data can also be impacted by interferences from other molecules or their fragments at key  $m/z$  values. For example, carry-over from the wet chemistry experiments (MTBSTFA, TMAH and/or their solvents and reaction products) can contribute signal to  $m/z$  28 (the main  $m/z$  of CO) and  $m/z$  30 (the main  $m/z$  of NO) as described below. In addition to carry-over from the wet chemistry analyses, there has been a MTBSTFA background resulting from a leak in at least one of the wet chemistry cups present since landing. Importantly, this background has been investigated and described in several works (Freissinet et al., 2015; Glavin et al., 2013; Stern et al., 2015; Sutter et al., 2017).

The EGA signal at  $m/z$  28 can be ascribed to the evolution of CO, but  $m/z$  28 can also have contributions from CO produced as an MS fragment of  $CO_2$  as well as signal from ethane, formaldehyde and methyl propene products of MTBSTFA (expected based on laboratory work studying MTBSTFA products, Stern et al., 2015) and methanol (byproduct from TMAH wet chemistry experiments). These additional contributions must be subtracted from the  $m/z$  28 signal to derive the signal indicative of evolved CO. Corrections for methanol ( $m/z$  31) were carried out only for data from the Groken sample (*italics below*) because methanol in SAM's background occurred after the TMAH wet chemistry analysis of the Mary Anning three (MA3) sample (Millan et al., 2022; Williams et al., 2021) and Groken was analyzed after that experiment.

The  $m/z$  28 signal from the CO MS fragment of  $CO_2$  was determined by assuming that this CO fragment from  $CO_2$  can be represented by the  $m/z$  28// $m/z$  45 ratio observed in evolved  $CO_2$  detected during EGA analyses of a calcite standard in SAM before launch as detailed in Archer et al. (2014) and Sutter et al. (2017). For ethane, methyl propene, and methanol (for Groken), the NIST ratios of  $m/z$  28// $m/z$  25,  $m/z$  28// $m/z$  39, and  $m/z$  28// $m/z$  31, respectively, were used to correct for  $m/z$  28 contributions from those phases (NIST Mass Spectrometry Data Center & Wallace, 2019).

To determine  $m/z$  28 from formaldehyde, first the below equation was used to obtain  $m/z$  29 attributable to formaldehyde:

$$m/z\ 29_{\text{Formaldehyde}} = m29 - m39 * 0.243 - m25 * 6.149 - (m31 * 0.446)_{\text{Groken only}}$$

This  $m/z$  29 was then multiplied by the  $m/z$  28// $m/z$  29 ratio from NIST (NIST Mass Spectrometry Data Center & Wallace, 2019) for formaldehyde. The values for  $m/z$  28 obtained for ethane, methyl propene, methanol (for Groken), and formaldehyde by this method, and the  $m/z$  28 obtained for the CO fragment of  $CO_2$ , were then subtracted from the original  $m/z$  28 signal to obtain a signal representing evolved CO. This correction is described in the below equation:

$$\text{CO} = m/z 28 - m45 * 3.2 - m25 * 28.6 - m39 * 0.49 - m29_{\text{Formaldehyde}} * 0.24 - (m31 * 0.046)_{\text{Groken only}}$$

To obtain an  $m/z$  30 signal representing NO evolved, we used a method discussed in Navarro-González et al. (2019) to correct for several MTBSTFA products that introduce mass interferences at  $m/z$  30. The  $m/z$  29 signal attributable to formaldehyde ( $m/z$  29<sub>Formaldehyde</sub> derived above) was used to determine expected interferences from formaldehyde and  $m/z$  43 signals were used to determine interferences from alkylaldehydes, ketones, or other hydrocarbons. These interference values are subtracted from the original  $m/z$  30 signal, as described by this equation:

$$\text{NO} = m/z 30 - 0.8 * (m/z 29_{\text{Formaldehyde}} - m/z 43)$$

Likewise, in order to plot a signal for H<sub>2</sub>S (main  $m/z$  34) evolved during SAM EGA, contributions to  $m/z$  34 from the <sup>34</sup>S isotopologue of the SO<sub>2</sub> S fragment must be subtracted. The  $m/z$  34 signal attributed to the SO<sub>2</sub> fragment is obtained by multiplying the  $m/z$  64 signal from the sample by the  $m/z$  34/ $m/z$  64 ratio in SO<sub>2</sub> evolved from a melanterite (FeSO<sub>4</sub>\*7H<sub>2</sub>O) calibration standard analyzed by SAM EGA before launch. This contribution is then subtracted from the total  $m/z$  34 signal to plot evolved H<sub>2</sub>S. This correction is further detailed in Archer et al. (2014) and Sutter et al. (2017). The equation used to derive H<sub>2</sub>S signal is:

$$\text{H}_2\text{S} = m/z 34 - (m/z 64 * (m/z 34/m/z 64)_{\text{melanterite std}})$$

In Section 5, evolved gas abundances are presented in terms of moles, moles/mg, and weight percent. Determination of the abundances of SO<sub>2</sub> and H<sub>2</sub>O was based on release of these gases during heating of a known mass of the hydrated Fe sulfate mineral melanterite in the SAM flight model prior to launch. Reported CO<sub>2</sub> abundances were based on CO<sub>2</sub> release during heating of a known mass of a calcite standard in SAM before launch. For other volatiles no prelaunch SAM data from standards exists, so literature values of the ionization cross sections for these molecules were used. These calculations are detailed in Archer et al. (2014). One difference in the abundance determinations discussed in Archer et al. (2014) and other SAM EGA focused manuscripts (e.g., Sutter et al., 2017) and the abundance approach used here is that changes in the drilling and sample delivery approach have occurred that have impacted estimates of delivered sample mass and error on that delivered sample mass. This newer drilling and sample delivery method is described further below in Section 4.3.

### 4.3. Sample Collection and Delivery

In this work we discuss SAM analyses of samples drilled from 5 locations in GT (Figures 1–3). Samples from these locations were also analyzed with the CheMin instrument. The Kilmarie (KM) sample was drilled from the Jura member. Two holes were drilled into KHm rocks at the Glen Etive (GE) site, largely driven by the need to obtain additional GE sample for SAM's MTBSTFA wet chemistry experiment. The GE1 and GE2 samples discussed here were from the first GE drill hole, and the GE3 sample was from the second GE drill hole. The MA samples, obtained from two drill holes at the MA site, are also from the KHm. The series of MA samples were obtained partly because of a mission desire to perform further SAM wet chemistry analyses in GT rocks before leaving GT, and GE-like materials present at the MA site were deemed most promising for these after analysis of data from GE. Two drill holes at MA were needed to acquire enough material for several SAM analyses including pyrolysis GCMS, MTBSTFA, and TMAH wet chemistry experiments, as well as CheMin analyses; the MA1 and MA2 samples discussed here were from the first drill hole. The Groken (GR) sample was acquired from an outcrop in the KHm nearby the MA site (~1 m away) which was targeted because of unusual diagenetic features including Mn- and P-rich dark nodules (Gasda et al., 2022). The Glasgow sample was drilled from the stratigraphically higher rocks of the Gm. An additional sample, Hutton (HU), was drilled from GT rocks near the contact between GT and the overlying Greenheugh pediment, and analyzed by SAM; the results of EGA analysis of this sample will be presented in a follow-on publication.



**Figure 3.** Mars Hand Lens Imager (MAHLI) images of the Glen Torridon drill holes from which the samples discussed here were obtained. Each hole is approximately 1.6 cm in diameter. Kilmarie (MAHLI image: 2404MH0007740010900288C00) was drilled from the Jura member. Glen Etive (2524MH0007740010903140C00), Glen Etive 2 (2550MH0007740010903254C00), Mary Anning (2851MH0001970011003289C00), and Groken (2920MH0004240011003512C00) were drilled from the Knockfarril Hill member. Glasgow (2773MH0004240011002826C00) was drilled from the Glasgow member. NASA/JPL-Caltech/MSSS.

The drilling approach used to obtain and deliver samples to SAM (and CheMin) was the same as that used during Curiosity's VRR campaign, and is termed feed-extended sample transfer (FEST). With FEST, drilled sample fines were stored in the drill stem, and this was vibrated and rotated to deliver subsamples of drilled fines to SAM cups through inlets in the rover deck (Fraeman et al., 2020). Sample fines from KM were delivered to cups in SAM's Oven #1 ring. Fines for analyses of two GE subsamples, runs that are here termed GE1 and GE2, were delivered to SAM's Oven #2 ring. A third SAM EGA run of a GE subsample, termed GE3, was run in Oven #1. MA (MA1 and MA2), GR and GG (GG1 and GG2) subsamples were also run in Oven #1.

#### 4.4. Subsample Mass Estimation

A combination of CheMin-derived sample mineralogy and processing of SAM EGA data was utilized to estimate the sample mass that SAM received from FEST delivery for a given run. This approach was detailed in McAdam et al., 2020 but, in summary, delivered sample mass estimates were based on abundances of minerals detected by CheMin that also were expected to release gases during SAM pyrolysis (i.e., phyllosilicates or hydrated Ca sulfates such as bassanite or gypsum which release H<sub>2</sub>O during pyrolysis). This was carried out by deconvolving SAM EGA traces, in this case H<sub>2</sub>O traces, into several peaks. Peaks at temperatures consistent with thermal decomposition of phyllosilicates or hydrated Ca sulfates were ascribed to those phases. The amount of H<sub>2</sub>O in peaks attributed to a given mineral was assumed to derive from the wt. % of that mineral obtained from CheMin data. Determination of the moles of H<sub>2</sub>O evolved in a given mineral's EGA peak and the moles of H<sub>2</sub>O expected from a given wt. % of phyllosilicate or hydrated Ca sulfate based on CheMin data were used together to estimate the mass of sample analyzed by SAM.

#### 4.5. Alpha Particle X-Ray Spectrometer Analyses

MSL's Alpha Particle X-ray Spectrometer (APXS) instrument enabled determination of the bulk chemistry of drilled rock powders delivered to SAM, by analyzing drill fines dropped from the drill bit or drill tailings (e.g., O'Connell-Cooper et al., 2022). In APXS analyses, a combination of alpha particles and X-rays are used to excite emission of characteristic X-rays from the elements in a sample. Total S and Cl measured by APXS (O'Connell-Cooper et al., 2022) were compared to SAM EGA S and Cl abundances to assess what fraction of total S and Cl was attributed to SAM EGA detected phases. Additional information about the APXS instrument and its analyses are discussed elsewhere (Campbell et al., 2012, 2014; Gellert et al., 2006, 2015).



## 5. Results and Interpretation

SAM analyses of GT samples resulted in evolved H<sub>2</sub>O, SO<sub>2</sub>, CO<sub>2</sub>, CO, NO, HCl, H<sub>2</sub>, and H<sub>2</sub>S. We focus on results from H<sub>2</sub>O, SO<sub>2</sub>, CO<sub>2</sub>, CO, NO, and HCl in the main text to discuss constraints on GT paleoenvironments, but H<sub>2</sub> and H<sub>2</sub>S EGA data and associated interpretation is included in the Supporting Information.

### 5.1. H<sub>2</sub>O

Water was evolved from all samples, and in several the amounts evolved were in higher abundances than previous Murray formation samples. The H<sub>2</sub>O abundances evolved ranged from ~0.8 to 3 wt. % (Table 1). Although several other phases including the enigmatic amorphous component of all samples contribute to evolved water, these overall higher abundances are likely related to evolutions from the clay minerals present in GT samples at the highest abundances observed in the mission so far (up to ~34 wt. % (Thorpe et al., 2022)). All samples released water as a broad release between ~100°C and ~550°C, but the H<sub>2</sub>O traces showed differences in peaks superimposed on the broad release (Figure 4), and several H<sub>2</sub>O traces also exhibited small peaks at temperatures above ~550°C (Figure 5).

Some water observed in all samples at temperatures below ~200°C can result from adsorbed water (e.g., Wang et al., 2011) and/or hydrated Ca sulfate (e.g., bassanite) present in several samples. KM1 (but not clearly observed in KM2), GE subsample runs, and GR have relatively sharp peaks between 100°C and 200°C (Figure 4), which likely results from dehydration of the hydrated Ca sulfate (bassanite) detected by CheMin in subsamples of the KM, GE, and GR targets (Thorpe et al., 2022). While their traces do not have a discrete peak, some of the H<sub>2</sub>O evolved at similar temperatures from MA and GG samples could result from the bassanite detected by CheMin in samples of MA and GG (Thorpe et al., 2022). All GT samples were inferred to contain amorphous or trace Fe sulfates, and some also amorphous or trace Mg sulfates, based on SO<sub>2</sub> evolutions during SAM analyses (discussed below in Section 5.2) and these salts can also release water at low temperatures. Other X-ray amorphous materials, such as opaline silica, poorly crystalline secondary silicate/aluminosilicate materials (e.g., allophane), nanophase iron oxyhydroxide minerals, altered glasses (e.g., palagonites), and volcanic glasses can dehydrate and/or dehydroxylate to evolve water over a span of temperatures including low temperatures. CheMin detected X-ray amorphous material in all GT samples (Thorpe et al., 2022) which likely consists of a mixture of different components including some of those listed above.

In all samples, small H<sub>2</sub>O peaks superimposed on the broader evolution between 200 and 300°C are notable (Figure 4). These are not straightforward to attribute to a specific well-crystalline phase detected by CheMin but could potentially result from a trace (present at abundances below CheMin detection limits) or poorly ordered (part of the X-ray amorphous component) goethite-like material in the samples.

The EGA H<sub>2</sub>O traces support the identification of Fe-rich dioctahedral 2:1 phyllosilicates, likely smectites (e.g., nontronite), from analysis of CheMin XRD data from all samples. H<sub>2</sub>O evolved between ~350°C and ~550°C in EGA traces (Figure 4) indicated that the samples contain a very Fe-rich dioctahedral phyllosilicate, such as the smectite nontronite, based on comparison to data from SAM-like lab EGA analyses of a range of phyllosilicates (e.g., McAdam et al., 2017) as well as expected trends in smectite dehydroxylation with differences in structures and octahedral chemistry (e.g., summarized in McAdam et al., 2020).

KM1, GE subsamples, GG subsamples, and GR show additional low intensity peaks in their EGA traces between ~600°C and 750°C (Figure 5). These EGA peaks may result from a mixed-layer serpentine/Fe-talc phase (S-T) dominated by Fe-talc or a mixed layer greenalite/minnesotaite phase (G-M) dominated by minnesotaite (MacKenzie et al., 1986), two mixed layer phases proposed for those samples (Bristow et al., 2021; Thorpe et al., 2022). While the dehydroxylation of other phyllosilicates can also be consistent with those release temperatures (e.g., montmorillonites, some illite-smectites), the observed low intensity H<sub>2</sub>O EGA peak was consistent with the CheMin detection of small amounts of S-T or G-M.

The H<sub>2</sub>O EGA traces from the MA subsamples both exhibited a very low intensity high temperature peak at ~820°C. If this peak derives from phyllosilicate dehydroxylation, it was consistent with very small amounts of an Mg-rich trioctahedral smectite such as saponite or endmember Mg-talc based on comparisons to data from EGA runs of several phyllosilicate reference materials under SAM-like conditions in the lab (McAdam et al., 2017).

**Table 1**  
*Abundances of Volatiles Evolved During SAM EGA and Total SO<sub>3</sub> and Cl Detected by APXS*

Sample	Kilmarie (KM1)		Kilmarie (KM2)		Glen Etive (GE1)		Glen Etive (GE2)		
Drill sol	2,384		2,384		2,486		2,486		
Analysis sol	2,393		2,398		2,497		2,499		
Molar Abundances									
Volatile	Units	$\mu$ or nmol	nmol/mg	$\mu$ or nmol	nmol/mg	$\mu$ or nmol	nmol/mg	$\mu$ or nmol	nmol/mg
CO <sub>2</sub>	$\mu$ mol	11.2 ± 2.7	294 ± 85	3.5 ± 0.5	253 ± 75	13.0 ± 3.4	97 ± 46	6.8 ± 1.2	123 ± 64
SO <sub>2</sub>	$\mu$ mol	3.48 ± 1.20	91.7 ± 28.8	0.7 ± 0.03	46.5 ± 13.3	11.59 ± 0.43	86.6 ± 39.6	2.5 ± 0.21	45.8 ± 23.7
H <sub>2</sub> O	$\mu$ mol	59.3 ± 25.7	1,561 ± 532	19.9 ± 10.0	1,423 ± 541	121.3 ± 72.2	906 ± 494	41.6 ± 34.4	750 ± 495
O <sub>2</sub>	$\mu$ mol	n.d. <sup>a</sup>	n.d.	n.d.	n.d.	n.d.	n.d.	n.d.	n.d.
H <sub>2</sub>	$\mu$ mol	12.4 ± 1.3	326 ± 88	12.8 ± 1.4	918 ± 267	15.7 ± 1.7	117 ± 54	9.6 ± 2.4	173 ± 92
HCl	nmol	273 ± 45	7.2 ± 2.0	72 ± 32	5.1 ± 1.9	3,509 ± 1,556	26.2 ± 13.3	1,132 ± 433	20.4 ± 11.2
H <sub>2</sub> S	nmol	92.6 ± 10.7	2.4 ± 0.7	25.0 ± 4.1	1.8 ± 0.5	225.9 ± 29.4	1.7 ± 0.8	114.0 ± 12.6	2.1 ± 1.1
CO	nmol	789 ± 44	20.8 ± 5.6	509 ± 28	36.4 ± 10.6	1,601 ± 86	12.0 ± 5.5	1,666 ± 90	29.7 ± 15.5
NO	nmol	n.d.	n.d.	n.d.	n.d.	6.7 ± 0.7	0.1 ± 0.02	1.3 ± 0.1	0.02 ± 0.01
Weight %									
CO <sub>2</sub>		1.29 ± 0.37		1.11 ± 0.36		0.43 ± 0.20		0.54 ± 0.30	
SO <sub>3</sub>		0.73 ± 0.23		0.37 ± 0.11		0.69 ± 0.32		0.37 ± 0.19	
H <sub>2</sub> O		2.81 ± 1.0		2.56 ± 0.97		1.63 ± 0.9		1.35 ± 0.89	
Cl <sub>2</sub> O <sub>7</sub>		n.d.		n.d.		n.d.		n.d.	
Cl		0.026 ± 0.007		0.018 ± 0.007		0.09 ± 0.05		0.07 ± 0.04	
Sample mass (mg)									
		38 ± 10		14 ± 4		134 ± 61		56 ± 29	
APXS wt. % (drill fines) <sup>b</sup>									
SO <sub>3</sub>		12.92 ± 0.15				4.13 ± 0.05			
Cl		0.32 ± 0.01				0.49 ± 0.02			
Sample	Glen Etive (GE3)		Mary Anning (MA1)		Mary Anning (MA2)		Groken (GR)		
Drill sol	2,527		2,838		2,838		2,910		
Analysis sol	2,531		2,844		2,850		2,918		
Molar Abundances									
Volatile	Units	$\mu$ or nmol	nmol/mg	$\mu$ or nmol	nmol/mg	$\mu$ or nmol	nmol/mg	$\mu$ or nmol	nmol/mg
CO <sub>2</sub>	$\mu$ mol	3.3 ± 1.4	20 ± 15	15.4 ± 3.1	136 ± 54	14.1 ± 3.4	134 ± 54	27.7 ± 7.5	309 ± 49
SO <sub>2</sub>	$\mu$ mol	5.7 ± 0.8	34.7 ± 25.5	11.05 ± 0.42	97.6 ± 37.4	11.0 ± 0.45	105.3 ± 40.6	9.87 ± 1.55	109.8 ± 12.8
H <sub>2</sub> O	$\mu$ mol	71.6 ± 21.6	433 ± 343	157.4 ± 98.6	1,390 ± 688	143.3 ± 82.3	1,369 ± 658	153.0 ± 94.4	1,703 ± 545
O <sub>2</sub>	$\mu$ mol	n.d.	n.d.	n.d.	n.d.	n.d.	n.d.	n.d.	n.d.
H <sub>2</sub>	$\mu$ mol	3.7 ± 0.7	22 ± 16	14.8 ± 2.8	131 ± 52	14.8 ± 2.8	141 ± 56	22.0 ± 4.2	245 ± 31
HCl	nmol	1,997 ± 779	12.1 ± 9.1	6,469 ± 2,685	57.2 ± 24.9	4,672 ± 7,118	44.6 ± 38.1	916 ± 334	10.2 ± 2.1
H <sub>2</sub> S	nmol	119.8 ± 13.6	0.7 ± 0.5	253.0 ± 39.3	2.2 ± 0.87	282.5 ± 33.1	2.7 ± 1.1	239.9 ± 65.0	2.7 ± 0.43
CO	nmol	678 ± 38	4.1 ± 3.0	1,024 ± 57	9.1 ± 3.5	1,243 ± 69	11.8 ± 4.6	2,957 ± 165	32.9 ± 3.5
NO	nmol	n.d.	n.d.	n.d.	n.d.	n.d.	n.d.	n.d.	n.d.
Weight %									
CO <sub>2</sub>		0.1 ± 0.1		0.60 ± 0.24		0.59 ± 0.27		1.36 ± 0.22	

**Table 1**  
*Continued*

Sample	Glen Etive (GE3)	Mary Anning (MA1)	Mary Anning (MA2)	Groken (GR)	
SO <sub>3</sub>	0.3 ± 0.21	0.78 ± 0.30	0.84 ± 0.33	0.88 ± 0.10	
H <sub>2</sub> O	0.8 ± 0.6	2.50 ± 1.2	2.46 ± 1.18	3.07 ± 1.0	
Cl <sub>2</sub> O <sub>7</sub>	n.d.	n.d.	n.d.	n.d.	
Cl	0.04 ± 0.03	0.20 ± 0.09	0.16 ± 0.14	0.04 ± 0.01	
Sample mass (mg)	165 ± 121	113 ± 43	105 ± 40	90 ± 8	
APXS wt. % (drill fines) <sup>b</sup>					
SO <sub>3</sub>	13.17 ± 0.15		9.60 ± 0.10	11.33 ± 0.123	
Cl	0.71 ± 0.02		0.91 ± 0.02	0.50 ± 0.02	
Sample	Glasgow (GG1)		Glasgow (GG2)		
Drill sol	2,752		2,752		
Analysis sol	2,765		2,771		
Molar Abundances					
Volatile	Units	μ or nmol	nmol/mg	μ or nmol	nmol/mg
CO <sub>2</sub>	μmol	4.5 ± 4.0	34 ± 22	4.5 ± 2.5	45 ± 25
SO <sub>2</sub>	μmol	16.9 ± 1.7	126.2 ± 59.8	18.1 ± 1.8	178.1 ± 86.6
H <sub>2</sub> O	μmol	123.9 ± 99.7	926 ± 574	76.7 ± 66.1	757 ± 490
O <sub>2</sub>	μmol	n.d.	n.d.	n.d.	n.d.
H <sub>2</sub>	μmol	6.6 ± 1.2	49 ± 24	5.1 ± 1.0	50 ± 25
HCl	nmol	4,896 ± 2,127	36.6 ± 19.0	5,330 ± 2,343	52.6 ± 27.9
H <sub>2</sub> S	nmol	248.1 ± 39.5	1.9 ± 0.9	249.3 ± 29.3	2.5 ± 1.2
CO	nmol	2,062 ± 115	15.4 ± 7.3	3,367 ± 187	33.3 ± 16.3
NO	nmol	6.5 ± 0.7	0.0 ± 0.02	n.d.	n.d.
Weight %					
CO <sub>2</sub>			0.15 ± 0.10	0.20 ± 0.15	
SO <sub>3</sub>			1.01 ± 0.48	1.43 ± 0.70	
H <sub>2</sub> O			1.67 ± 1.0	1.36 ± 0.88	
Cl <sub>2</sub> O <sub>7</sub>			n.d.	n.d.	
Cl			0.13 ± 0.07	0.19 ± 0.10	
Sample Mass (mg)			134 ± 63	101 ± 49	
APXS wt. % (drill fines) <sup>b</sup>					
SO <sub>3</sub>			7.48 ± 0.15		
Cl			1.12 ± 0.04		

Note. Errors on molar abundances are 2-sigma errors, and errors on nmol/mg abundances are 1-sigma errors.

<sup>a</sup>n.d.: not detected. <sup>b</sup>From O'Connell-Cooper et al., 2022.

## 5.2. SO<sub>2</sub>

All samples released SO<sub>2</sub> between ~400°C and 700°C, consistent with S derived from Fe sulfates and/or Fe sulfides (Figure 6). The abundance of evolved SO<sub>2</sub> varied from ~0.3 wt. % (GE3) to ~1.4 wt. % (GG2) (Table 1). Detections of OCS, CS<sub>2</sub> and other key evolved volatiles as well as the isotopic composition of evolved SO<sub>2</sub> suggest that one of the samples, KM, may contain some reduced sulfur (Wong et al., 2022).

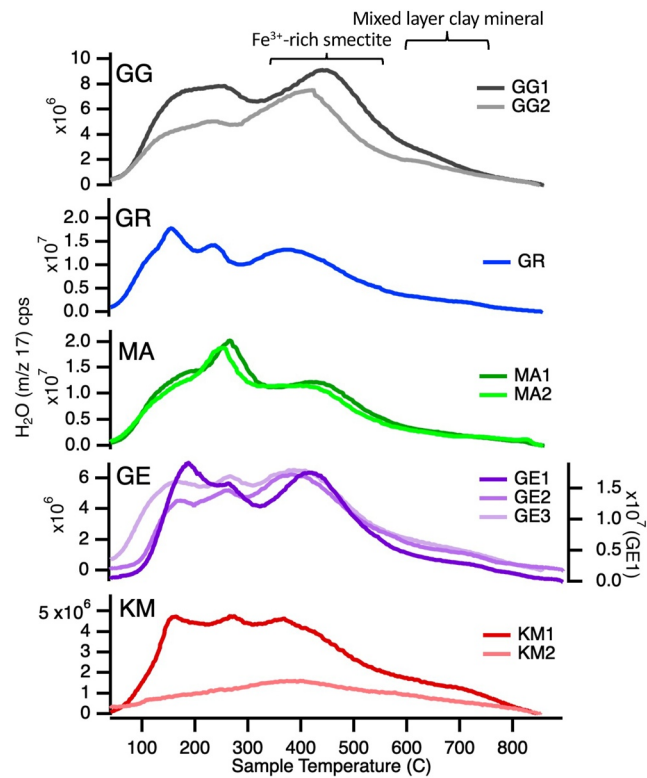


**Figure 4.** H<sub>2</sub>O signal versus temperature from SAM EGA of GT samples. Brackets denote the temperature ranges of H<sub>2</sub>O evolution expected from clay minerals in the samples.

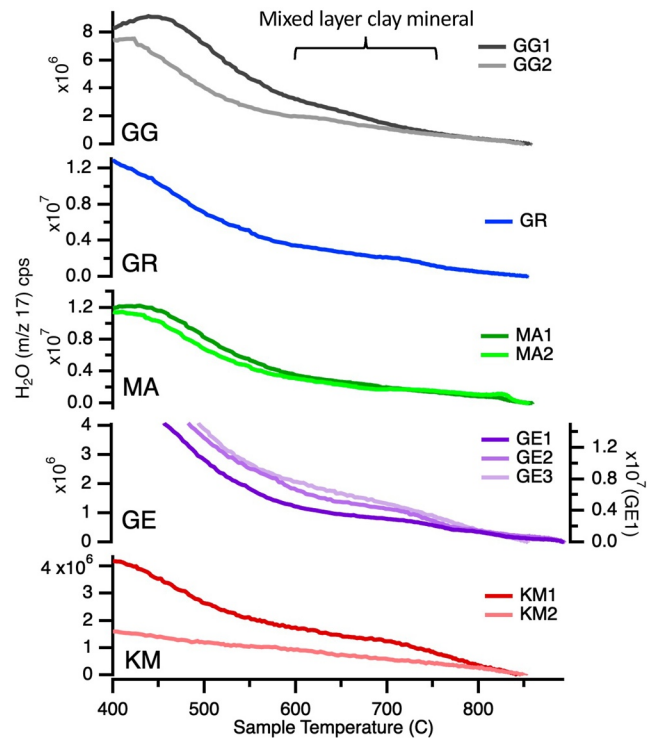


**Figure 5.** Signal from H<sub>2</sub>O evolved at temperatures above 400°C during SAM EGA of GT samples. This view of H<sub>2</sub>O EGA traces enables low intensity peaks evolved between ~600°C and 750°C in Kilmarie, Glen Etive, Glasgow and Groken samples to be more clearly seen.

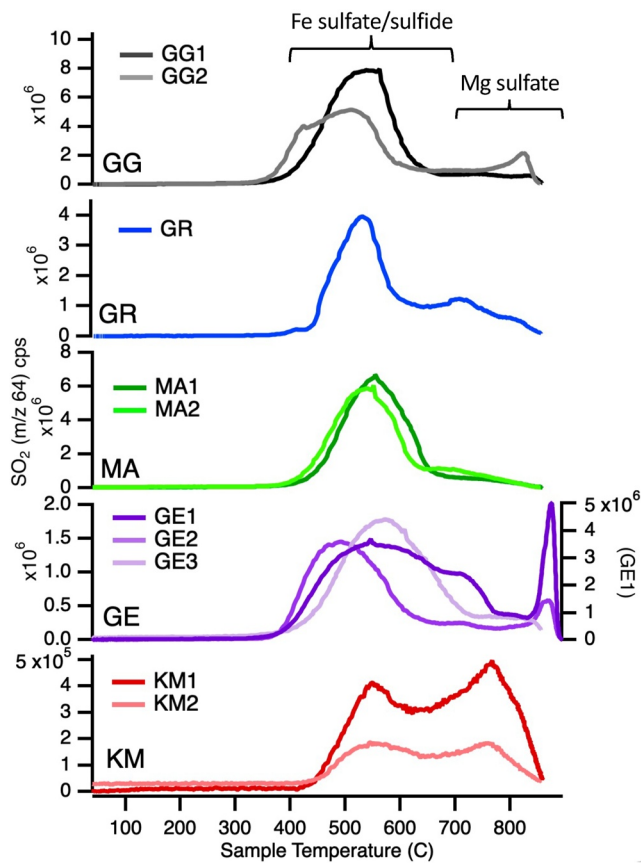


**Figure 6.** SO<sub>2</sub> signal versus temperature from SAM EGA of GT samples. Brackets denote expected SO<sub>2</sub> evolution temperatures for relevant sulfur minerals.

The KM subsamples and the GE1 and GE2 subsamples evolved significant SO<sub>2</sub> at temperatures >~700°C, while GE3, GR and GG had smaller SO<sub>2</sub> releases and MA evolved very little above ~700°C (Figure 6). The >~700°C evolutions are consistent with Mg sulfate decomposition in the presence of other phases. Individually, when heated under SAM-like conditions, Mg sulfates will begin to release SO<sub>2</sub> near the end of the SAM oven temperature range. However, when together with other materials, for example, chloride phases, Mg sulfate can evolve SO<sub>2</sub> at lower temperatures and this process is considered to be an important contributor to SO<sub>2</sub> evolved at temperatures above 700°C (McAdam et al., 2016; Mu & Perlmutter, 1981; Sutter et al., 2017 and references therein). The differences in the intensity of the SO<sub>2</sub> signal at temperatures above 700°C for the GT samples were attributed to a difference in the abundances of Mg sulfates in the samples, indicating that the KM and GE targets contained the most Mg sulfate (though GE exhibited variation between the GE drill sample subsamples, and between samples from the two different drill holes), and MA, GR, and GG contained less Mg sulfate.

No crystalline Fe sulfates/sulfides or Mg sulfates were detected by CheMin XRD analysis (Thorpe et al., 2022) indicating that Fe sulfate/sulfides and Mg sulfates inferred from SAM data are present at abundances below CheMin's detection limit and/or are X-ray amorphous. Mg sulfates (and Fe sulfates) can be expected to be amorphous under many martian conditions (e.g., Sklute et al., 2015; Vaniman et al., 2014). Sulfur can also be present in X-ray amorphous sulfides, S-bearing inclusions in glass or other amorphous materials, or sulfate anions adsorbed onto materials (McAdam et al., 2014; Rampe et al., 2016). S-bearing organic compounds are another potential host for trace amounts of sulfur in the samples, and in fact SAM GCMS analyses indicate a large diversity of S-bearing organics in several GT samples (Millan et al., 2022).

The Fe and Mg sulfates indicated by SAM SO<sub>2</sub> EGA data make up a small fraction of the total S present in the GT samples as detected by APXS (Table 1). Most samples analyzed by SAM have also shown this trend (e.g.,

Knudson et al., 2018; Sutter et al., 2017) indicating that Ca sulfate phases dominate the S mineralogy in Gale crater, as detected by CheMin (e.g., Rampe et al., 2017, 2020; Thorpe et al., 2022). Sulfur in Ca sulfates was generally not detected during SAM EGA analyses because Ca sulfates thermally decompose at higher temperatures than those achieved during SAM pyrolysis.

### 5.3. CO<sub>2</sub>

The abundances of CO<sub>2</sub> evolved from GT samples varied from ~0.1 wt. % (GE3) to ~1.4 wt. % (GR) (Table 1). Most CO<sub>2</sub> evolved between ~200°C and ~550°C, with small amounts evolved below ~200°C and above ~550°C (Figure 7). The CO<sub>2</sub> evolved from these samples can have contributions from adsorbed CO<sub>2</sub>, carbonate, oxidized organic compounds and oxidation of reduced organics (in the SAM instrument background or indigenous to the sample) during heating.

Evolved CO<sub>2</sub> traces from all GE samples and the GG1 sample were broader than those from the MA, GR, and KM samples which evolved CO<sub>2</sub> as a sharper peak (Figure 7). CO<sub>2</sub> evolved above ~400°C in EGA data can be attributed to siderite decomposition (Sutter et al., 2017). It is also possible for siderite to start decomposing at temperatures as low as ~300°C if it is finely crystalline (Archer et al., 2013, 2020). It may be that a significant amount (but not all, see below) of the 300°C–500°C CO<sub>2</sub> evolved from GT samples was from siderite. Siderite was detected by CheMin in the KM, GE, MA, and GR samples. For most samples, except for the GG samples and the GE3 sample in which no siderite was detected by CheMin, the CO<sub>2</sub> expected from the CheMin-detected amount of siderite was a significant fraction of the total SAM evolved CO<sub>2</sub> (Figure 8).

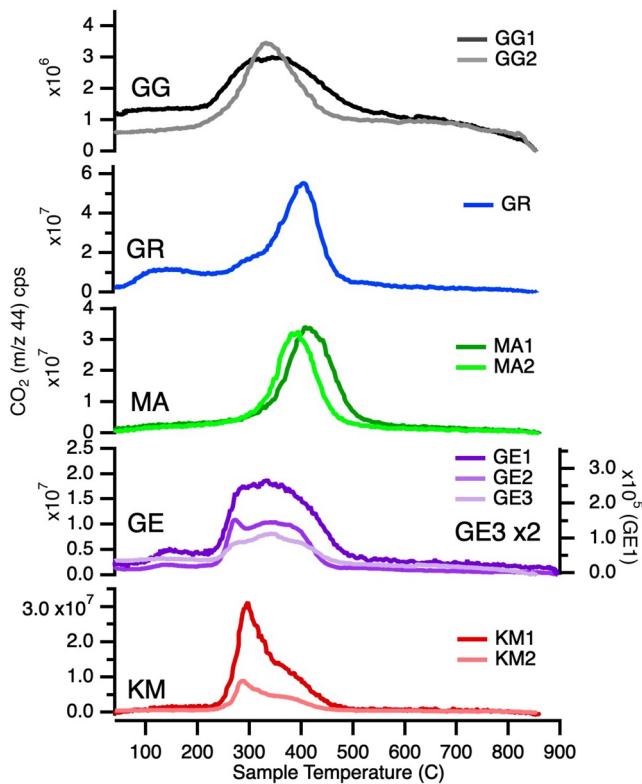


**Figure 7.** CO<sub>2</sub> signal versus temperature from SAM EGA of GT samples. Evolutions are consistent with siderite and oxidized carbon compounds such as oxalates.

Thermal decomposition of oxidized organic compounds (e.g., oxalates Applin et al., 2015; Franz et al., 2020; Lewis et al., 2021), and oxidation of reduced organics (SAM background or indigenous to the sample) during heating, also possibly contributed CO<sub>2</sub> at a range of temperatures including in the 200°C–550°C range. For most samples where CheMin detected siderite, there was still excess SAM CO<sub>2</sub> (even considering the error bars), so that siderite cannot account for all the CO<sub>2</sub>. Importantly, this is also consistent with the details of the CO<sub>2</sub> EGA traces, in which some CO<sub>2</sub> evolves below 300°C which is too low for siderite decomposition. The overlaps of part or most of the CO<sub>2</sub> evolution temperatures with CO evolution temperatures (Section 5.4) for some samples also supports the possible presence of some oxidized organics such as oxalate salts (e.g., Applin et al., 2015; Franz et al., 2020; Lewis et al., 2021) (these oxidized organics evolve CO<sub>2</sub> and CO at similar temperatures during pyrolysis but carbonates generally do not). Oxidized carbon phases such as oxalates are anticipated components of martian surface materials, expected from oxidation or irradiation of reduced organic compounds derived from meteoritic infall or endogenous to Mars (e.g., Benner et al., 2000). Finally, it is also possible that slightly more or less evolved CO<sub>2</sub> than expected from CheMin-derived siderite abundances shown in Figure 8 can be attributed to error on CheMin abundances for trace minerals or, likely more importantly, the fact that CheMin does not analyze exactly the same sample as SAM. CheMin and SAM receive subsamples of a given drill sample and while the mineralogy is expected to be very similar between subsamples there may be some heterogeneity in the detailed mineralogy including the siderite abundances.

The only samples that evolved significant CO<sub>2</sub> above 550°C were the GG samples. These broad releases may have contributions from very minor Mg

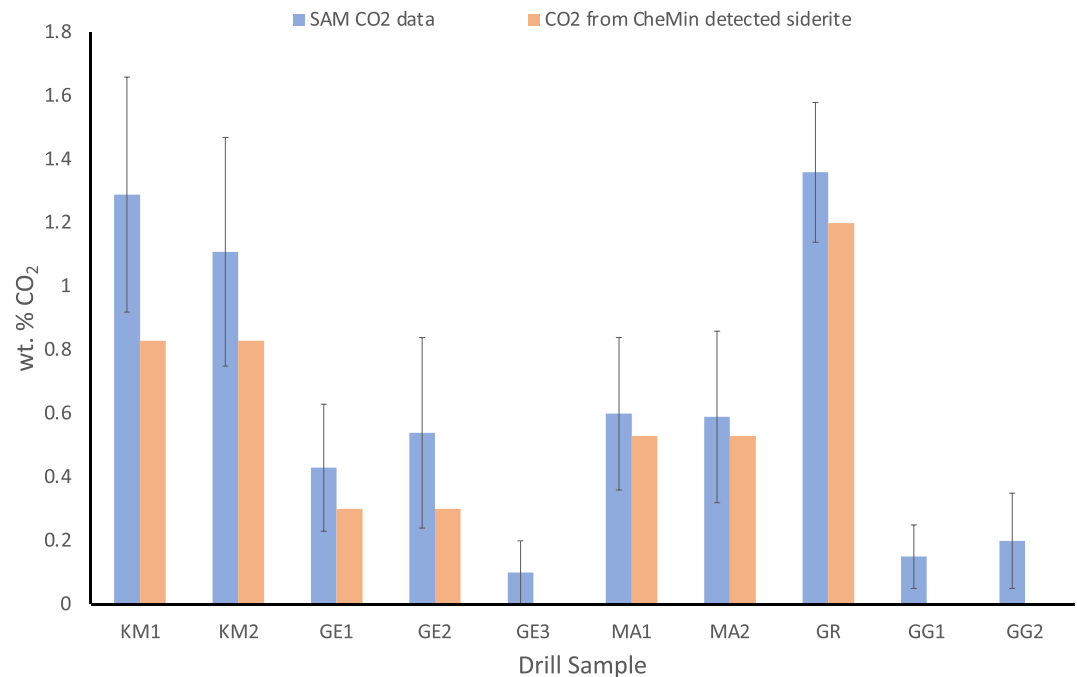


**Figure 8.** Abundances of CO<sub>2</sub> evolved from all GT samples during SAM EGA compared to the amount expected from thermal decomposition of CheMin-detected abundances of siderite (Thorpe et al., 2022) in those samples. For most samples, except for the GG samples and the GE3 sample where no siderite was detected by CheMin, the CO<sub>2</sub> expected from the CheMin-detected amount of siderite is a significant fraction of the total SAM evolved CO<sub>2</sub>.

or Ca carbonates, and/or oxidized organic compounds.  $\text{CO}_2$  released below  $\sim 200^\circ\text{C}$  was thought to result from adsorbed  $\text{CO}_2$  (e.g., Janchen et al., 2009) and/or the oxidation of organic compounds in the SAM instrument background (e.g., wet chemistry byproducts, see Section 4.2). The broad  $< 200^\circ\text{C}$  peak in GR is an example where contributions from the SAM background are especially likely, as the GR sample run followed the two wet chemistry runs on MA samples (which contributed wet chemistry reagents to the background) and plots of the  $m/z$  signal consistent with several wet chemistry by-products show peaks at similar temperatures. As mentioned above, it is also possible that oxidation of organics in the SAM background contributed some  $\text{CO}_2$  at temperatures above  $200^\circ\text{C}$ . This is discussed in more detail in Section 5.4 as a possible contributor to some of the  $\text{CO}$  evolutions observed in the  $\sim 200^\circ\text{C}$ – $550^\circ\text{C}$  range in GT sample runs, but it could also be a factor in some of the observed  $\text{CO}_2$ .

#### 5.4. CO

The abundances of evolved  $\text{CO}$  ranged from  $\sim 4$  nmol/mg ( $\sim 115$  ppm) to  $\sim 36$  nmol/mg ( $\sim 1,019$  ppm) (Table 1).  $\text{CO}$  evolutions (Figure 9) largely overlapped with the temperatures of  $\text{CO}_2$  evolutions in the case of KM, GE, GG (Figure 7) but were offset to lower temperatures for MA and GR. The majority of  $\text{CO}$  was evolved from  $\sim 200^\circ\text{C}$  to  $500^\circ\text{C}$ , but some  $\text{CO}$  was evolved at temperatures higher than  $550^\circ\text{C}$  as well; MA exhibited small peaks between  $\sim 650^\circ\text{C}$  and  $700^\circ\text{C}$  and GE1, GE2, and GG2 exhibited small peaks above  $800^\circ\text{C}$  (Figure 9).

The thermal decomposition, decarboxylation, and decarbonylation of oxidized carbon phases such as organic salts (e.g., oxalates) in the samples were possible contributors to evolved  $\text{CO}$  (and  $\text{CO}_2$ ) (e.g., Lewis et al., 2021). Many oxalates evolve  $\text{CO}$  and  $\text{CO}_2$  at the same temperatures, so samples where those evolutions largely overlapped were the most likely to have contained them. Also, the amount of evolved  $\text{CO}$  compared to the amount of evolved  $\text{CO}_2$  during pyrolysis can broadly inform as to the likelihood of geologically-relevant oxalate species contributing to evolved  $\text{CO}$  and  $\text{CO}_2$  (e.g., Lewis et al., 2021). In all samples except for GG, the amount of  $\text{CO}$  evolved was much lower than the amount of  $\text{CO}_2$  evolved. If the  $\text{CO}$  did predominantly derive from oxidized organic compounds such as oxalates, this could indicate more of these compounds being present in GG.

Another possible contributor to observed  $\text{CO}$  (and  $\text{CO}_2$ ) was partial oxidation of reduced organics by evolved oxygen or other compounds during heating in the SAM ovens. As discussed in Section 5.5 below, no evolved oxygen was detected from the GT samples but a small amount of  $\text{O}_2$  could have been evolved from the samples and subsequently scrubbed, before detection by the MS, by reaction with reduced organics in the oven to form  $\text{CO}$  (and possibly also lesser  $\text{CO}_2$ ).

Small  $\text{CO}$  peaks seen above  $550^\circ\text{C}$  (Figure 9) could derive from relatively refractory organic compounds (e.g., macromolecular carbon material) that undergo decarbonylation or decarboxylation at high temperature (e.g., Eigenbrode et al., 2018). These peaks in GE1, GE2, and GG2 also overlap with evolutions of high temperature  $\text{SO}_2$  (Figure 6) from those samples. This may indicate that the  $\text{CO}$  was related to the oxidation of reduced C that was trapped within or otherwise associated with a sulfate and released/oxidized when the sulfate decomposed (Francois et al., 2016).  $\text{OCS}$  and  $\text{CS}_2$  evolved coincident with the high temperature  $\text{CO}$  and  $\text{SO}_2$  in the GE1 run also support this idea of reduced C present and available to react with S species. These sorts of associations between organics and sulfates have been discussed as possibilities for past samples analyzed by SAM (e.g., Eigenbrode et al., 2018; Freissinet et al., 2019) and sulfur-bearing organics detected in SAM GCMS runs of GT samples, including GG and GE, may also indicate associations or interactions between sample reduced organic compounds and sulfates or  $\text{SO}_2$  evolved during their decomposition (Millan et al., 2022).

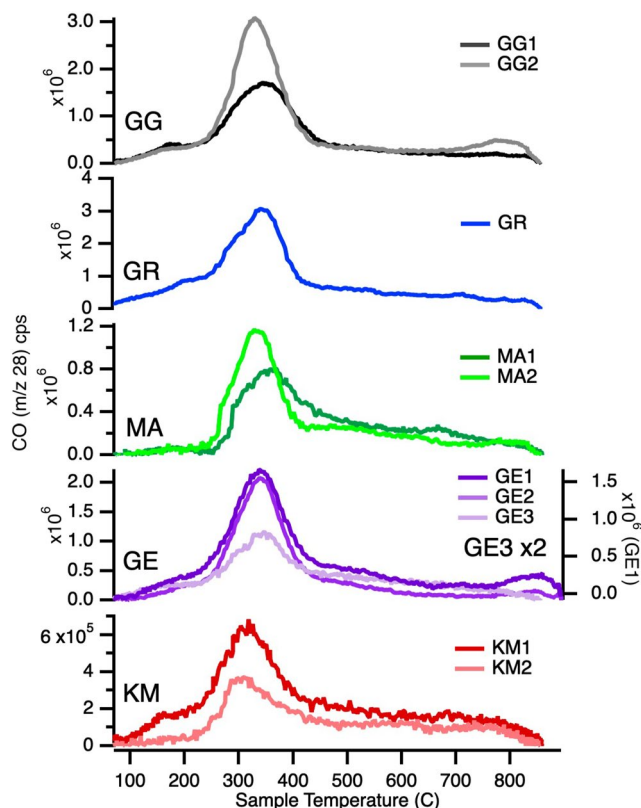


**Figure 9.** Evolved  $\text{CO}$  signal versus temperature. Possible sources include thermal decomposition of oxidized organic compounds (e.g., oxalates) and oxidation of reduced organics—either in the SAM background or indigenous to the sample. Contributions from oxidation of the SAM background are less likely at higher temperatures.

EGA signals attributed to SAM background materials can be observed from most samples at temperatures below 550°C but are generally not prevalent at higher temperatures. This may suggest that CO evolved below ~550°C requires careful consideration of contributions from oxidation of SAM background organics but that this source is more unlikely at higher temperatures.

### 5.5. O<sub>2</sub>

No O<sub>2</sub> was evolved from any of the GT samples. O<sub>2</sub> evolved during other SAM EGA runs, for example, of the RH sample of the Jura on VRR (McAdam et al., 2020), was ascribed to thermal decomposition of oxychlorine phases such as perchlorate and chlorate salts (e.g., Glavin et al., 2013; Hogancamp et al., 2018; Sutter et al., 2017). A lack of O<sub>2</sub> evolution is inferred to suggest a lack of oxychlorine salts, and other minerals that produce O<sub>2</sub> on heating, in the analyzed sample, though it is possible that detectable levels of oxygen were released but then consumed during SAM pyrolysis by reactions with organics (to produce CO/CO<sub>2</sub> as discussed above) and/or minerals (e.g., reaction of O<sub>2</sub> with magnetite to produce hematite) before detection.

The lack of evolved O<sub>2</sub> can also offer a potential constraint on GR sample mineralogy. The GR drill area is known to be generally enriched in Mn (the MnO abundance detected in the GR drill sample by APXS was  $1.07 \pm 0.03$  wt. %, O'Connell-Cooper et al., 2022). One possible host would be trace or amorphous Mn oxides (Mn oxides were not detected by CheMin), and Mn can occur in several oxidation states in oxides. SAM-like lab analyses of a variety of Mn oxides demonstrated that thermal decomposition of Mn<sup>3+</sup> and Mn<sup>4+</sup> oxides evolve O<sub>2</sub> while Mn<sup>2+</sup> oxides do not (Clark et al., 2021). This suggests that any Mn oxides present in GR occurred as Mn<sup>2+</sup> oxides.

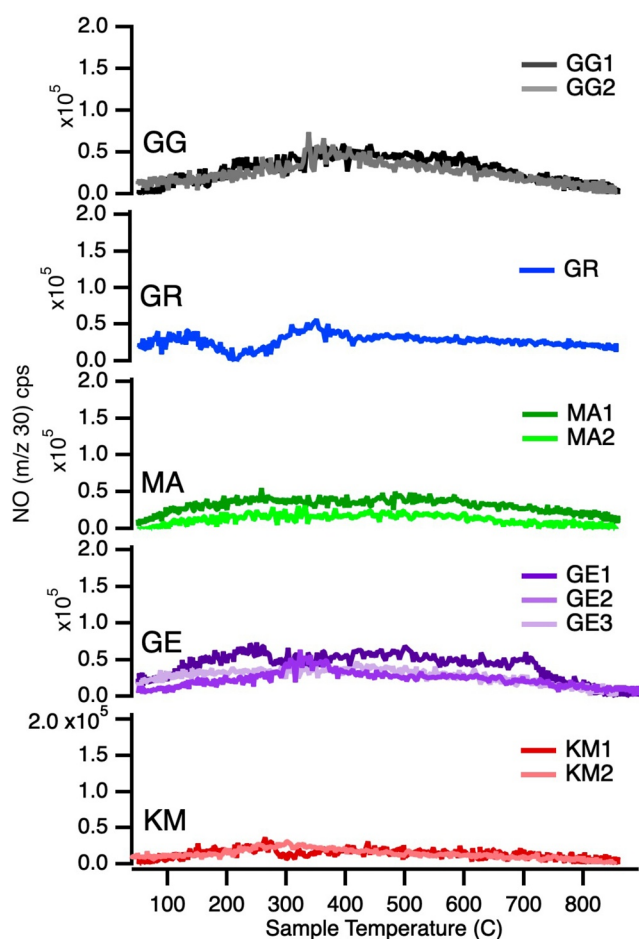


**Figure 10.** NO EGA signal versus temperature. The lack of significant NO releases suggests no, or very little, nitrate or nitrite salts are present in GT samples.

### 5.6. NO

Similar to measurements of evolved O<sub>2</sub>, there was also very little or no NO evolved from all the GT samples. Very small releases of NO were observed during the GE1, GE2, and GG1 runs (Table 1), over a generally similar temperature range, with all three runs showing weak NO evolutions between ~200°C and ~450°C, but GE1 also exhibited a weak 700°C peak not observed in GE2 and GG1 runs (Figure 10). NO evolved during other SAM EGA runs, for example, the RH VRR sample, was attributed to the likely thermal decomposition of trace nitrate or nitrite salts in the samples, though other sources of N could also contribute to NO production (Andrejkovičová et al., 2018). The ~200°C to ~450°C NO evolutions from GE1, GE2, and GG1, if from very small amounts of nitrate/nitrite salts, would be consistent with Fe nitrate or Fe nitrite based on runs of these salts in the lab using SAM-like parameters (Navarro-González et al., 2019; Stern et al., 2015).

### 5.7. HCl

The amount of HCl evolved by the GT samples varied significantly, with KM and GR samples evolving the least total HCl (~5–10 nmol/mg, or ~180–360 ppm) and MA1 evolving the most (~57 nmol/mg, or ~2,050 ppm) (Table 1). The overall shapes of the HCl EGA traces were similar for the GE, MA, and GG samples, with a rise at ~300°C followed by a wide evolution though in detail the intensity of this evolution varied (Figure 11). The small amount of HCl evolved from the KM samples produced a low intensity trace with few distinct features, while the somewhat larger but still fairly small amount of total HCl evolved from GR generated an HCl trace with a distinct peak at very high temperatures near 780°C.

In all of the discussed samples, HCl observed could derive its Cl from trace chlorides in the samples. Chlorides can undergo reactions with water or other evolved gases during the SAM pyrolysis to give HCl as a product (Clark,



Sutter, McAdam, Rampe, et al., 2020; Sutter et al., 2017 and references therein). No Cl minerals, including chlorides, were detected during CheMin analyses of the GT samples (Bristow et al., 2021; Thorpe et al., 2022) suggesting that if chlorides are present their abundances are below CheMin detection limits. The very broad HCl evolutions spanning to high temperatures, most prominent in GE, MA, and GG samples (Figure 11), are consistent with the shape of HCl traces obtained during lab SAM-like EGA of chlorides in mixtures with some water-evolving phases (e.g., mixtures of NaCl and nontronite) (Clark, Sutter, McAdam, Rampe, et al., 2020).

NaCl can result in HCl release at high temperatures (Clark, Sutter, McAdam, Rampe, et al., 2020). This can likely be traced to its melting temperature, and other sample minerals (e.g., sulfates) and evolved gases can affect HCl evolution behavior (Clark, Sutter, McAdam, Archer, et al., 2020; Clark, Sutter, McAdam, Rampe, et al., 2020). The distinct peak at  $\sim 780^\circ\text{C}$  in the GR HCl trace, and the peak at similar temperatures in the MA2 HCl trace superimposed on the broader release, could result from molten or partially molten NaCl, given that its melting temperature is similar (Westphal et al., 1997), or possibly from an Mn-chloride which is also expected to produce HCl at similar temperatures. The GR sample site was known to be enriched in Mn which drives our suggestion of this possibility for GR, but Mn chloride or any chloride present is present in trace abundances not detectable by CheMin.

HCl could also be produced by trace amounts of other Cl-bearing minerals present below CheMin detection limits, such as akaganeite detected in past samples analyses (e.g., akaganeite in the RH sample, Rampe et al., 2020 and the Cumberland (CB) sample, Vaniman et al., 2014), but if so, distinct HCl peaks in the expected temperature range ( $\sim 400\text{--}700^\circ\text{C}$ , Peretyazhko et al., 2019) must be obscured by other HCl release. Oxychlorine phases, inferred present in several past samples analyzed by SAM (e.g., RH, McAdam et al., 2020 and CB, Ming et al., 2014) are unlikely to be present and contributing HCl since no evolved  $\text{O}_2$  was observed during analyses of the GT samples (Section 5.5).

For all of the GT samples, APXS detected more wt. % Cl than was observed in SAM evolved HCl (Table 1). Trace chlorides are the likely source for this Cl since the HCl released from chlorides during heating can be incomplete leaving unreacted Cl (because the amount of HCl released is strongly affected by reactions during heating). If the excess Cl detected by APXS but not SAM is equated with abundances of the lightest likely chloride (NaCl) or the heaviest potential chloride discussed ( $\text{MnCl}_2$ ), some samples (MA, GG) have Cl equivalent to slightly more than 1 wt. % chlorides which would likely be above CheMin detection limits (although chlorides were not observed by CheMin). This indicates that the Cl is in multiple Cl-bearing phases or that chlorides or other Cl-bearing phases are X-ray amorphous, or both.

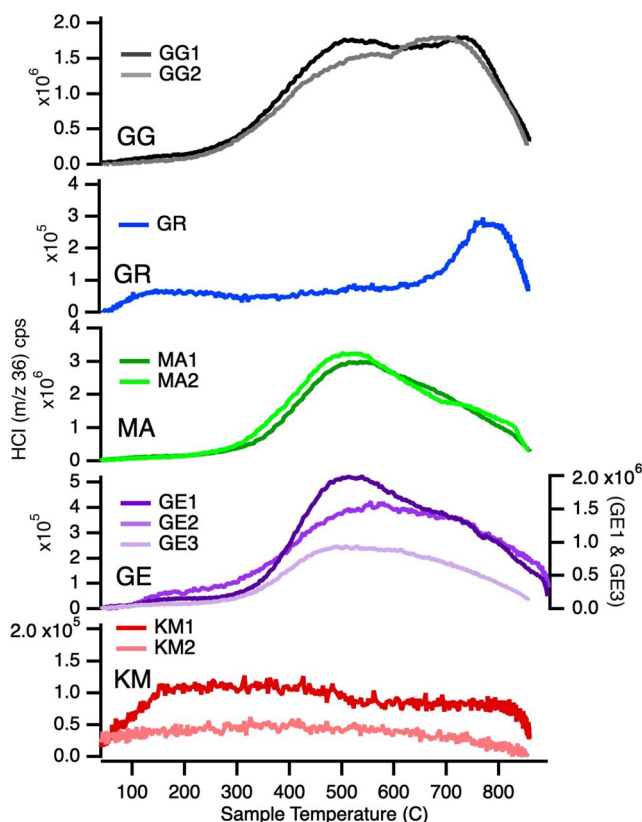


**Figure 11.** HCl EGA signal versus temperature. The HCl likely derives from reactions with trace chlorides present in all samples.

## 6. Discussion

Several inputs and constraints on the geochemistry and mineralogy of the Jm, KHm and Gm in GT have been enabled by SAM analyses. SAM EGA data: (1) support the Fe-rich and dioctahedral nature of smectite clay minerals identified by CheMin in all GT samples, (2) bolster the inference of trace mixed layer S-T or G-M in several GT samples, (3) support the presence of trace siderite in several GT samples (KM, GE, MA, GR), (4) enable the inference of trace or amorphous Fe sulfates in all GT samples (and possible Fe sulfides in KM) and trace/amorphous Mg sulfates in some GT samples (mainly KM and GE samples), (5) indicate the likely absence of oxychlorine salts and  $\text{Mn}^{3+}$  and  $\text{Mn}^{4+}$  oxides, (6) indicate very little or no nitrate/nitrite salts, (7) reveal the presence of oxidized organics, and (8) imply the presence of trace chloride salts in GT samples. This information can be used, together with chemical, mineralogical, stratigraphic and textural data obtained by MSL, to inform the conditions of sediment deposition and alteration that have influenced GT rocks.

### 6.1. Redox Potential of Alteration Fluids

The detection of siderite ( $\text{Fe}^{2+}$  carbonate),  $\text{Fe}^{2+}$ -phyllosilicates, and sulfides indicated that reducing alteration conditions had occurred in GT sediments. Siderite inferred from SAM EGA data and observed with CheMin in Jm and KHm rocks indicated a fluid environment with low redox potential. SAM EGA data also suggest some carbonate may be present in the VRR Jura at RH (McAdam et al., 2020), but if so it is very trace (below CheMin detection limits) (Rampe et al., 2020). If the 9.2 Å phase detected by CheMin and supported by SAM data from Jm and several KHm rocks was an  $\text{Fe}^{2+}$ -bearing mixed layer clay mineral (e.g., G-M or S-T), these minerals further suggest interaction with reduced alteration fluids during deposition or post-depositional alteration if they are authigenic or in sediment source regions if they are detrital. Reduced sulfur, probably in trace authigenic sulfides, inferred from SAM data to be present in the KM sample of the GT Jura (Wong et al., 2022) and the Jura exposed on VRR (Wong et al., 2020), also points to reducing conditions. An authigenic origin may be more likely than input of detrital igneous sulfides during deposition of the original basaltic detritus in the GT sediment's fluvial/lacustrine environment because SAM evidence of sulfides has been relatively uncommon but was present in the VRR and parts of GT closest to VRR. In addition, in the case of the GT Jura, the  $\delta^{34}\text{S}$  of  $\text{SO}_2$  EGA peaks in the data from KM was more consistent with S from trace authigenic sulfides than S from igneous sulfides (Wong et al., 2022). The lack of  $\text{O}_2$  evolution in SAM EGA analyses indicated that if Mn oxides are hosts for some of the Mn observed in GT, such as at the Mn-rich site Groken in the KHm, the Mn in oxides remained as  $\text{Mn}^{2+}$  because most  $\text{Mn}^{3+}$  and  $\text{Mn}^{4+}$  oxides should have released  $\text{O}_2$  in SAM EGA analyses (Clark et al., 2021) and this was not observed. Finally, SAM GCMS and wet chemistry experiments on several GT samples revealed reduced carbon indigenous to the samples, in particular sulfur-bearing organics evolved at high pyrolysis temperatures (Millan et al., 2022).

Conversely, there were also minerals detected or inferred in GT materials that point to episodes of oxidizing alteration conditions. In some samples of the Murray formation analyzed by SAM earlier in the mission there were indications of both dioctahedral and Mg-bearing trioctahedral smectites (e.g., the Marimba sample (e.g., Achilles et al., 2020)). The dominance of  $\text{Fe}^{3+}$ -rich dioctahedral smectites in all GT samples, with little indication of trioctahedral smectites, indicates comparatively more oxidizing alteration conditions, either during syndepositional or post-deposition alteration of the GT sediments in place (if the smectites are authigenic) or during alteration in the sediment source or sediment transport processes (if smectites are detrital) (Bristow et al., 2018). Sulfate salts detected by SAM in all GT samples also point to oxidizing environments. Finally, oxidized organic compounds evidenced by SAM evolved  $\text{CO}_2$  and CO EGA data from all samples indicate oxidizing conditions.

### 6.2. Alteration Fluid Chemistry

Neutral or alkaline fluid interactions are indicated by the presence of substantial abundances of smectite clay minerals in all GT samples, as well as siderite in many of the samples. Siderite also implies sufficient carbonic acid, as well as low sulfur contents, in the fluids from which it formed (Garrels & Christ, 1965). At least some localized acidic fluid interactions (possibly associated with the oxidation of sulfides) were indicated by SAM  $\text{SO}_2$  EGA peaks pointing to the presence of trace/amorphous Fe sulfates in all GT samples and most VRR samples (McAdam et al., 2020). Amorphous/trace Mg sulfates were indicated by SAM EGA data from all VRR samples (McAdam et al., 2020) and in the KM and some GE samples but are either comparatively less abundant, or are not observed, in stratigraphically higher GT samples (KHm and Gm samples). This difference in Mg sulfate content with stratigraphy may result from heterogeneity in fluid chemistry over time. This may also imply that Mg sulfate was originally precipitated throughout GT but it was later partially leached from some KHm and Gm rocks (as represented by MA, GR, GG) where less Mg sulfate was detected.

### 6.3. Water-To-Rock Ratios (W/R)

The observation that GT phyllosilicates are dominated by dioctahedral smectites (with only minor G-M or S-T in some samples) points to relatively high W/R, more open system conditions compared to rocks analyzed earlier in the mission that contained trioctahedral or trioctahedral and dioctahedral smectites. This inference applies to in place syndepositional or diagenetic alteration of the GT sediments (for authigenic smectites) or alteration in source regions or during transport (for detrital smectites). The lack of highly soluble oxychlorine salts, and very trace or absent nitrate/nitrite salts, is also consistent with open system/leached conditions, provided they

were present at one time in the history of GT rocks. Chemical Index of Alteration (CIA) values from ChemCam instrument analyses of bedrock in GT also suggest a rock record of open system alteration (Dehouck et al., 2022).

On the other hand, there are also indications of some low W/R conditions in the history of GT sediments. SAM HCl data suggests soluble chloride salts remain in all GT samples. In addition, siderite is generally unstable under high W/R conditions.

#### 6.4. Plausible Series of Events

The constraints enabled by our current data do not facilitate determination of a unique set of processes recorded in GT, but we summarize in Figure 12 and discuss below a plausible series of episodes that accounts for the observations of GT and considers the context of GT rocks within the larger Murray including the nearby diagenetically altered VRR which contains Jura formation rocks that are also exposed in GT.

1. First, basaltic primary minerals, pyroxenes and feldspars, detected in the Jm, KHm and Gm in GT (Thorpe et al., 2022), as well as in the Jura member exposed on nearby VRR (Rampe et al., 2020), were detrital inputs to the depositional environment of GT and VRR sediments. The minor well-crystalline 9.2 Å phase detected by CheMin in some GT samples may have also been a detrital input (Bristow et al., 2021). Significant abundances of Fe<sup>3+</sup>-rich dioctahedral smectites, trace oxidized carbon compounds (e.g., oxalates), chlorides, trace/amorphous Fe sulfates, and notably variable amounts of trace/amorphous Mg sulfates detected in all VRR and GT samples were formed syn-depositionally or through alteration processes after lithification.
2. Next, siderite detected in Jm and KHm was deposited from a fluid environment with low W/R, relatively low sulfur, low redox potential, and near neutral pH but with sufficient carbonic acid likely resulting from interaction with Mars' CO<sub>2</sub> atmosphere. This could have occurred in a stage of the lake environment, perhaps during an evaporative event, a partial freezing event, or during later diagenesis. It is possible this siderite may have been originally more abundant than now observed in GT rocks, since it tends to be replaced by ferric iron oxyhydroxides and oxides, and/or Fe<sup>3+</sup>-bearing clay minerals if interacted with higher pH and more oxidizing

1. Basaltic primary minerals and possibly clay minerals (9.2 Å phase) were detrital inputs to the lacustrine/fluviol sediments of GT and VRR. Fe<sup>3+</sup>-rich dioctahedral smectites, trace oxidized carbon compounds (e.g., oxalates), chlorides, trace/amorphous Fe sulfates, and notably variable amounts of trace/amorphous Mg sulfates were formed in syn-depositional or post-depositional environments of variable W/R, chemistry and pH.  
(Affected VRR Jura, GT Jura, KHm, and Gm)



2. Siderite was deposited from fluids with low W/R, relatively low S, low redox potential, and near neutral pH but with sufficient carbonic acid. This siderite may have been originally more abundant, then partially replaced by Fe oxyhydroxides/oxides and/or Fe-bearing clay minerals. Oxidized carbon phases remained in the sediments. If the trace 9.2 Å phase is authigenic, it could have precipitated from the same fluid as the siderite.  
(Affected GT Jura, KHm)



3. Reduced S, probably in trace sulfides, in GT Jura and VRR Jura was precipitated during fluid interactions that affected both VRR Jura and the adjacent GT Jura. Chloride may have been partially removed but oxidized carbon phases were not impacted.  
(Affected VRR Jura, GT Jura)



4. Alteration event(s) reduced phyllosilicate abundances, formed additional hematite and amorphous silica/aluminosilicate materials, and changed the structure of phyllosilicates in VRR Jura compared to GT Jura.  
(Affected VRR Jura)



5. Very late-stage fluids delivered trace oxychlorine and nitrate/nitrite salts to the VRR Jura site RH and Stimson rocks but interactions were patchy and did not affect GT samples.

**Figure 12.** A plausible sequence of events that have influenced the alteration history of Glen Torridon (GT) and its context within adjacent materials such as the Vera Rubin ridge (VRR).

- fluids (Gasda et al., 2022). This process could have also contributed to the heterogeneity in siderite abundances now observed in Jm and KHm rocks. If the 9.2 Å phase is an authigenic clay mineral such as mixed layer G-M hypothesized by Thorpe et al. (2022) the siderite may have been deposited from the same fluids as formed the G-M, since these minerals are known to occur together in terrestrial settings.
- Then, reduced sulfur, probably in trace sulfides, in the GT Jura (Wong et al., 2022), and the Jura exposed on VRR (Wong et al., 2020), may have been formed during a fluid event associated with the alteration of the VRR Jura that also affected the adjacent GT Jura. The sulfides could be formed, for example, by disproportionation of sulfite in sulfite-bearing fluids, as hypothesized by Wong et al. (2020) for the VRR sulfides. This event may have also resulted in the relatively low abundances of HCl-evolving phases indicated by SAM EGA analyses of the GT Jura and VRR Jura samples (McAdam et al., 2020) compared to other GT samples.
  - An alteration event or events affected the Jura member exposed on VRR but not the Jura member exposed in GT. The stratigraphic equivalence of these units that also displayed significant differences in observed mineralogy and chemistry enabled a unique opportunity for insights into the complex history recorded in these and adjacent Murray units. This event(s) leads to a reduction in the original phyllosilicate content, and results in the precipitation of significant additional hematite and amorphous silica and aluminosilicate materials. SAM H<sub>2</sub>O EGA data was consistent in that it indicates less H<sub>2</sub>O from phyllosilicate dehydroxylation in VRR Jura samples versus GT Jura samples. There were also indications of differences in the structure of phyllosilicates in the VRR Jura compared to GT Jura (Rampe et al., 2020). One idea (e.g., McAdam et al., 2020; Rampe et al., 2020) was that the phyllosilicate in VRR Jura was a ferripyrophyllite resulting from interaction with warm, saline and slightly acidic fluids. Thorpe et al. (2022) hypothesized that the VRR Jura phyllosilicates were minnesotaite or nontronite close in composition to minnesotaite. SAM H<sub>2</sub>O EGA data from the VRR Jura samples Rockhall (RH) and Highfield (HF) are consistent with both ferripyrophyllite and nontronite which are both Fe-rich dioctahedral 2:1 phyllosilicates with similar dehydroxylation temperature <550°C–600°C (McAdam et al., 2020).
  - Very late-stage fluids delivered trace oxychlorine and nitrate/nitrite salts to the VRR Jura site RH and the Stimson rocks of the Greenheugh pediment, as evidenced by O<sub>2</sub> and NO evolved from RH and Greenheugh pediment samples. These interactions were patchy and did not affect GT samples. The other possibility is that interaction with oxychlorine and nitrate/nitrite bearing fluids was more pervasive but that very soluble oxychlorine and nitrate/nitrite salts precipitated in GT samples were then leached out by a later fluid. If this was the case, however, these fluids either left soluble chloride salts which are inferred from SAM data to still be present in all GT samples or chloride salts were precipitated during a later fluid event.

## 7. Summary and Implications

SAM EGA analyses have enabled several constraints and inputs on the mineralogy and chemistry of GT rocks drilled by Curiosity. The temperatures of H<sub>2</sub>O evolutions in SAM EGA data supported the idea that the major phyllosilicate present in all of the GT samples was an Fe-rich dioctahedral smectite, and were also consistent with the presence of lesser amounts of a phyllosilicate such as mixed layer talc-serpentine or mixed layer greenalite-minnesotaite. The dominance of Fe<sup>3+</sup>-rich dioctahedral smectites in the GT rocks, compared to some earlier Murray formation rocks which contained indications of both dioctahedral and Mg-bearing trioctahedral smectites (e.g., Achilles et al., 2020), indicated a continuing trend toward progressively more open system and oxidizing alteration environments up section in the Murray (Bristow et al., 2018). This alteration could have occurred at or near the time of sediment deposition or during post-depositional alteration, producing the dioctahedral smectites authigenically, but it is also possible they are detrital and reflect alteration conditions in their source region or during transport. SAM CO<sub>2</sub> EGA data supported the detection of trace siderite in several GT drill samples (KM, GE, MA, GR) by CheMin (Bristow et al., 2021; Thorpe et al., 2022). Trace and/or amorphous Fe sulfur phases were inferred to be present in all samples, with these likely being sulfate in all GT samples except KM which may contain some Fe sulfides (Wong et al., 2022). In contrast, significant indications of trace/amorphous Mg sulfates were only observed in two GT samples (KM and GE samples). The lack of O<sub>2</sub> evolution in SAM EGA analyses indicated the probable absence of minerals such as Mn<sup>3+</sup> and Mn<sup>4+</sup> oxides and oxychlorine salts. The lack of, or very minor amount of, NO evolved pointed to absent or very trace nitrate/nitrite salts. The nature of SAM HCl EGA curves overall suggested the presence of trace chloride salts in GT samples. Trace abundances of oxidized carbon compounds such as oxalate salts may be indicated by CO and some CO<sub>2</sub> evolution during EGA of several GT samples. SAM pyrolysis GCMS and wet chemistry experiments

also detected reduced organic compounds in several GT samples, and the reader is referred to Millan et al. (2022) for a detailed discussion of those results.

The constraints above can be used to inform the redox potential, chemistries, and fluid-to-rock ratio conditions of a complex and variable set of past GT fluid events. The presence of siderite, Fe<sup>2+</sup>-bearing mixed layer clay minerals, sulfides, Mn<sup>2+</sup> oxides, and potential reduced carbon (Millan et al., 2022) in the samples indicated a reducing fluid episode or episodes. The presence of smectites dominated by dioctahedral Fe<sup>3+</sup>-bearing smectites and oxidized organic compounds pointed to oxidizing fluid event(s). Substantial abundances of smectite clay minerals in all GT samples, and siderite, imply neutral/alkaline fluid conditions, while at least some small-scale acidic fluid interactions are suggested by trace/amorphous Fe sulfate. Siderite also indicated sufficient carbonic acid and low amounts of sulfur in the fluids from which it precipitated. Differences in the amounts of amorphous/trace Mg sulfates throughout GT indicate heterogeneity in alteration fluid sulfate chemistry. Alteration episodes under relatively open system, high W/R conditions are inferred from abundant smectites in GT samples, as well as a lack or near lack of highly soluble oxychlorine and nitrate/nitrite salts. However, the presence of soluble chloride salts in all GT samples, and siderite in several samples, suggested some low W/R fluid events.

We presented a possible series of events which may have influenced the rocks of GT and the adjacent VRR. First, basaltic detritus (and possibly also trace G-M or S-T) was deposited. Then, Fe<sup>3+</sup>-rich dioctahedral smectites, trace oxidized carbon compounds (e.g., oxalates), chlorides, trace/amorphous Fe sulfates, and variable amounts of trace/amorphous Mg sulfates were formed close to the time of sediment deposition or in post-depositional environments. Next, siderite was deposited in fluid environments with low W/R, relatively low S, reducing conditions, and near neutral pH but with sufficient carbonic acid. Trace G-M may have formed during the same fluid event that precipitated the siderite if it was authigenic. Then, reduced S, probably in trace sulfides, in GT Jura (Wong et al., 2022) and VRR Jura (Wong et al., 2020) formed during fluid interactions that affected both VRR Jura and the proximal GT Jura. Next, an alteration event or events affected the VRR Jura member but not the GT Jura. The event resulted in a reduction of the VRR Jura's phyllosilicate content, the precipitation of significant additional hematite and amorphous silica/aluminosilicate materials and changes to the structure of phyllosilicates compared to the GT Jura materials. Finally, a very late fluid event supplied trace oxychlorine and nitrate/nitrite salts to part of the VRR Jura, as represented by the RH site (McAdam et al., 2020), and the Stimson rocks of the Greenheugh pediment which overlies GT (Sutter et al., 2020) but these salts were not delivered to GT rocks.

Overall, SAM EGA data, in the context of additional mineralogy, chemistry, and textural data obtained by Curiosity, indicated that the integrated environmental history of GT and the adjacent VRR involved alteration with fluids of variable redox potential, chemistry and pH under a variety of fluid-to-rock ratios. This included alteration conditions enabling siderite precipitation, an environmental record not yet observed in rocks analyzed by Curiosity, alteration processes that produced the largest abundances of smectite clay minerals observed to date, and fluid interactions which did not favor formation/preservation of Mg sulfates in several sampled GT areas. Several of the indicated fluid episodes could have provided habitable environmental conditions. Carbon (detected by SAM in CO<sub>2</sub>, CO and reduced organic compounds) would have been available to any past microbes in Gale crater, but a lack of significant N in the near surface could have introduced a limiting factor. Curiosity is currently exploring the sulfate unit which overlies GT, and ongoing rover investigations will further elucidate the complex environmental history recorded in Gale crater's sedimentary rocks.

#### Acknowledgments

We thank the numerous scientists and engineers of the MSL and SAM teams without whom this manuscript would not be possible. We also thank members of the SAM and MSL team for their insightful inputs and support. The authors would like to remember and acknowledge thoughtful discussions about SAM data from Glen Torridon with Rafael Navarro-González, a dedicated SAM team member who passed away on 28 January 2021. In addition, we thank Adrian Broz, Walter Goetz, and JGR editor Deanne Rogers for their helpful review comments which improved this manuscript. A.C.M., J.L.E., and C.H.H. acknowledge funding support from the NASA ROSES MSL Participating Scientist Program. C.N.A. acknowledges support from the NASA Postdoctoral Program, administered by USRA through a contract with NASA.

#### Data Availability Statement

The data from SAM utilized in this manuscript is archived by EIDs (KM1: eid25515; KM2: eid25517; GE1: eid25530; GE2: eid25533; GE3: eid25538; MA1: eid25596; MA2: eid25600; GR: eid25622; GG1: eid25579; GG2: eid25582) and publicly available at NASA's Planetary Data System Geosciences Node (Mahaffy, 2013).

#### References

- Achilles, C. N., Rampe, E. B., Downs, R. T., Bristow, T. F., Ming, D. W., Morris, R. V., et al. (2020). Evidence for multiple diagenetic episodes in ancient fluvial-lacustrine sedimentary rocks in Gale crater, Mars. *Journal of Geophysical Research-Planets*, 125(8), e2019JE006295. <https://doi.org/10.1029/2019JE006295>
- Andrejkovičová, S., McAdam, A. C., Stern, J. C., Knudson, C. A., Navarro-González, R., Millan, M., et al. (2018). NH<sub>4</sub>-Smectite, a potential source of N compounds (NO) in SAM analyses. In *49th Lunar and Planetary Science Conference, Abstract #1998, The Woodlands, TX*.

- Applin, D. M., Izawa, M. R. M., Cloutis, E. A., Goltz, D., & Johnson, J. R. (2015). Oxalate minerals on Mars? *Earth and Planetary Science Letters*, *420*, 127–139. <https://doi.org/10.1016/j.epsl.2015.03.034>
- Archer, P. D., Franz, H. B., Sutter, B., Arevalo, R. D., Coll, P., Eigenbrode, J. L., et al. (2014). Abundances and implications of volatile-bearing species from evolved gas analysis of the Rocknest aeolian deposit, Gale Crater, Mars. *Journal of Geophysical Research: Planets*, *119*(1), 237–254.
- Archer, P. D., Ming, D. W., & Sutter, B. (2013). The effects of instrument parameters and sample properties on thermal decomposition: Interpreting thermal analysis data from Mars. *Planetary Science*, *2*, 1–21. <https://doi.org/10.1186/2191-2521-2-2>
- Archer, P. D., Rampe, E. B., Clark, J. V., Tu, V., Sutter, B., Vaniman, D., et al. (2020). Detection of siderite (FeCO<sub>3</sub>) in Glen Torridon samples by the Mars Science Laboratory rover. In *51st Lunar and Planetary Science Conference, Abstract #2709, The Woodlands, Texas*.
- Benner, S. A., Devine, K. G., Matveeva, L. N., & Powell, D. H. (2000). The missing organic molecules on Mars. *Proceedings of the National Academy of Sciences of the United States of America*, *97*, 2425–2430. <https://doi.org/10.1073/pnas.040539497>
- Bennett, K. A., Fox, V. K., Bryk, A., Dietrich, W., Fedo, C., Edgar, L., et al. (2022). The Curiosity Rover's Exploration of Glen Torridon, Gale crater, Mars: An Overview of the Campaign and Scientific Results. *Journal of Geophysical Research: Planets*, *127*, e2022JE007185. <https://doi.org/10.1029/2022JE007185>
- Bish, D. L., Blake, D. F., Vaniman, D. T., Chipera, S. J., Morris, R. V., Ming, D. W., et al. (2013). X-ray diffraction results from Mars Science Laboratory: Mineralogy of Rocknest at Gale crater. *Science*, *341*, 1238932. <https://doi.org/10.1126/science>
- Bristow, T. F., Bish, D. L., Vaniman, D. T., Morris, R. V., Blake, D. F., Grotzinger, J. P., et al. (2015). The origin and implications of clay minerals from Yellowknife Bay, Gale crater, Mars. *American Mineralogist*, *100*(4), 824–836. <https://doi.org/10.2138/am-2015-5077CCBYNCND>
- Bristow, T. F., Grotzinger, J. P., Rampe, E. B., Cuadros, J., Chipera, S. J., Downs, G. W., et al. (2021). Brine-driven destruction of clay minerals in Gale crater, Mars. *Science*, *373*(6551), 198–204. <https://doi.org/10.1126/science.abg5449>
- Bristow, T. F., Rampe, E. B., Achilles, C. N., Blake, D. F., Chipera, S. J., Grotzinger, J. P., et al. (2018). Clay mineral diversity and abundance in sedimentary rocks of Gale crater, Mars. *Science Advances*, *4*(6), eaar3330. <https://doi.org/10.1126/sciadv.aar3330>
- Calef, F. J., II, & Parker, T. (2016). *MSL Gale merged orthophoto mosaic (25 centimeter per pixel scale)*. NASA Planetary Data System (PDS) Annex, U.S. Geological Survey. Retrieved from [http://bit.ly/MSL\\_Basemap](http://bit.ly/MSL_Basemap)
- Campbell, J. L., King, P. L., Burkemper, L., Berger, J. A., Gellert, R., Boyd, N. I., et al. (2014). The Mars Science Laboratory APXS calibration target: Comparison of Martian measurements with the terrestrial calibration. *Nuclear Instruments and Methods in Physics Research Section B: Beam Interactions with Materials and Atoms*, *323*, 49–58. <https://doi.org/10.1016/j.nimb.2014.01.011>
- Campbell, J. L., Perrett, G. M., Gellert, R., Andrushenko, S. M., Boyd, N. I., Maxwell, J. A., et al. (2012). Calibration of the Mars Science Laboratory Alpha Particle X-ray Spectrometer. *Space Science Reviews*, *170*(1–4), 319–340. <https://doi.org/10.1007/s11214-012-9873-5>
- Clark, J. V., Lanza, N., Rampe, E. B., Archer, P. D., Morris, R. V., Tu, V., et al. (2021). Evolved gas analysis of manganese-bearing phases and implications for the Sample Analysis at Mars (SAM) instrument on board the Curiosity rover in Gale crater, Mars. In *52nd Lunar and Planetary Science Conference, Abstract #1209, Virtual*.
- Clark, J. V., Sutter, B., McAdam, A. C., Archer, P. D., Rampe, E. B., Ming, D. W., et al. (2020). High-temperature hydrogen chloride releases from mixtures of sodium chloride with sulfates: Implications for the chlorine-mineralogy as determined by the Sample Analysis at Mars instrument on the Curiosity rover in Gale crater, Mars. In *Paper Presented at the 51st Lunar and Planetary Science Conference, Abstract #1435, The Woodlands, Texas*.
- Clark, J. V., Sutter, B., McAdam, A. C., Rampe, E. B., Archer, P. D., Ming, D. W., et al. (2020). High-temperature HCl evolutions from mixtures of perchlorates and chlorides with water-bearing phases: Implications for the SAM instrument in Gale crater, Mars. *Journal of Geophysical Research-Planets*, *125*(2). <https://doi.org/10.1029/2019JE006173>
- Dehouck, E., Cousin, A., Mangold, N., Frydenvang, J., Gasnault, O., Forni, O., et al. (2022). Bedrock geochemistry and alteration history of the clay-bearing Glen Torridon region of Gale crater, Mars. *Journal of Geophysical Research: Planets*, *127*, e2021JE007103. <https://doi.org/10.1029/2021JE007103>
- Eigenbrode, J. L., Summons, R. E., Steele, A., Freissinet, C., Millan, M., Navarro-Gonzalez, R., et al. (2018). Organic matter preserved in 3-billion-year-old mudstones at Gale crater, Mars. *Science*, *360*(6393), 1096–1100. <https://doi.org/10.1126/science.aas9185>
- Farmer, J. D., & Des Marais, D. J. (1999). Exploring for a record of ancient Martian life. *Journal of Geophysical Research-Planets*, *104*(E11), 26977–26995. <https://doi.org/10.1029/1998je000540>
- Fedo, C. M., Bryk, A. B., Edgar, L. A., Bennett, K. A., Fox, V. K., Dietrich, W. E., et al. (2022). Geology and stratigraphic correlation of the Murray and Carolyn Shoemaker formations across the Glen Torridon region, Gale crater, Mars. *Journal of Geophysical Research: Planets*, *127*, e2022JE007408. <https://doi.org/10.1029/2022JE007408>
- Fedo, C. M., Grotzinger, J. P., Bryk, A., Edgar, L. A., Bennett, K., Fox, V., et al. (2020). Ground-based stratigraphic correlation of the Jura and Knockfarril Hill members of the Murray formation, Gale crater: Bridging the Vera Rubin ridge—Glen Torridon divide. In *51st Lunar and Planetary Science Conference, Abstract #2345, The Woodlands, Texas*.
- Fedo, C. M., Grotzinger, J. P., Gupta, S., Fraeman, A., Edgar, L., Edgett, K., et al. (2018). Sedimentology and Stratigraphy of the Murray Formation, Gale Crater, Mars. In the 49th Lunar and Planetary Science Conference, Abstract #2078. The Woodlands, Texas.
- Fox, V. K., Bennett, K. A., Bryk, A., Arvidson, R. E., Bristow, T., Dehouck, E., et al. (2020). One year in Glen Torridon: Key results from the Mars Science Laboratory Curiosity rover exploration of clay-bearing units. In *51st Lunar and Planetary Science Conference, Abstract #2833, The Woodlands, Texas*.
- Fraeman, A. A., Arvidson, R. E., Catalano, J. G., Grotzinger, J. P., Morris, R. V., Murchie, S. L., et al. (2013). A hematite-bearing layer in Gale crater, Mars: Mapping and implications for past aqueous conditions. *Geology*, *41*(10), 1103–1106. <https://doi.org/10.1130/G34613.1>
- Fraeman, A. A., Edgar, L. A., Rampe, E. B., Thompson, L. M., Frydenvang, J., Fedo, C. M., et al. (2020). Evidence for a diagenetic origin of Vera Rubin ridge, Gale crater, Mars: Summary and synthesis of Curiosity's exploration campaign. *Journal of Geophysical Research-Planets*, *125*(12), e2020JE006527. <https://doi.org/10.1029/2020JE006527>
- Fraeman, A. A., Ehlmann, B. L., Arvidson, R. E., Edwards, C. S., Grotzinger, J. P., Milliken, R. E., et al. (2016). The stratigraphy and evolution of lower Mount Sharp from spectral, morphological, and thermophysical orbital data sets. *Journal of Geophysical Research-Planets*, *121*(9), 1713–1736. <https://doi.org/10.1002/2016je005095>
- Francois, P., Szopa, C., Buch, A., Coll, P., McAdam, A. C., Mahaffy, P. R., et al. (2016). Magnesium sulfate as a key mineral for the detection of organic molecules on Mars using pyrolysis. *Journal of Geophysical Research-Planets*, *121*(1), 61–74. <https://doi.org/10.1002/2015je004884>
- Franz, H. B., Mahaffy, P. R., Webster, C. R., Flesch, G. J., Raaen, E., Freissinet, C., et al. (2020). Indigenous and exogenous organics and surface-atmosphere cycling inferred from carbon and oxygen isotopes at Gale crater. *Nature Astronomy*, *4*(5), 526. <https://doi.org/10.1038/s41550-019-0990-x>
- Freissinet, C., Glavin, D. P., Buch, A., Szopa, C., Teinturier, S., Archer, P. D., et al. (2019). Detection of long-chain hydrocarbons on Mars with the Sample Analysis at Mars (SAM) instrument. In *Ninth International Conference on Mars, Abstract #6123, LPI Contribution No. 2089, Lunar and Planetary Institute*.

- Freissinet, C., Glavin, D. P., Mahaffy, P. R., Miller, K. E., Eigenbrode, J. L., Summons, R. E., et al. (2015). Organic molecules in the Sheepbed Mudstone, Gale crater, Mars. *Journal of Geophysical Research-Planets*, 120(3), 495–514. <https://doi.org/10.1002/2014je004737>
- Garrels, R. M., & Christ, C. L. (1965). *Solutions, minerals and equilibria*. Harper and Row, New York
- Gasda, P. J., Comellas, J., Essunfeld, A., Das, D., Bryk, A. B., Dehouck, E., et al. (2022). Overview of the Morphology and Chemistry of Diagenetic Features in the Clay-Rich Glen Torridon Unit of Gale Crater, Mars. *Journal of Geophysical Research: Planets*, 127, e2021JE007097. <https://doi.org/10.1029/2021JE007097>
- Gellert, R., Clark, B. C., & MSL and MER Science Teams. (2015). In situ compositional measurements of rocks and soils with the Alpha Particle X-ray Spectrometer on NASA's Mars rovers. *Elements*, 11(1), 39–44. <https://doi.org/10.2113/gselements.11.1.39>
- Gellert, R., Rieder, R., Bruckner, J., Clark, B. C., Dreibus, G., Klingelhofer, G., et al. (2006). Alpha Particle X-ray Spectrometer (APXS): Results from Gusev crater and calibration report. *Journal of Geophysical Research-Planets*, 111(E2), E02s05. <https://doi.org/10.1029/2005je002555>
- Glavin, D. P., Freissinet, C., Miller, K. E., Eigenbrode, J. L., Brunner, A. E., Buch, A., et al. (2013). Evidence for perchlorates and the origin of chlorinated hydrocarbons detected by SAM at the Rocknest aeolian deposit in Gale Crater. *Journal of Geophysical Research-Planets*, 118(10), 1955–1973. <https://doi.org/10.1002/jgre.20144>
- Grotzinger, J. P., Crisp, J., Vasavada, A. R., Anderson, R. C., Baker, C. J., Barry, R., et al. (2012). Mars Science Laboratory mission and science investigation. *Space Science Reviews*, 170(1–4), 5–56. <https://doi.org/10.1007/s11214-012-9892-2>
- Grotzinger, J. P., Sumner, D. Y., Kah, L. C., Stack, K., Gupta, S., Edgar, L., et al. (2014). A habitable fluvio-lacustrine environment at Yellowknife Bay, Gale crater, Mars. *Science*, 343(6169). <https://doi.org/10.1126/science.1242777>
- Hogancamp, J. V., Sutter, B., Morris, R. V., Archer, P. D., Ming, D. W., Rampe, E. B., et al. (2018). Chlorate/Fe-bearing phase mixtures as a possible source of oxygen and chlorine detected by the Sample Analysis at Mars instrument in Gale crater, Mars. *Journal of Geophysical Research-Planets*, 123(11), 2920–2938. <https://doi.org/10.1029/2018je005691>
- Janchen, J., Morris, R. V., Bish, D. L., Janssen, M., & Hellwig, U. (2009). The H<sub>2</sub>O and CO<sub>2</sub> adsorption properties of phyllosilicate-poor palagonitic dust and smectites under martian environmental conditions. *Icarus*, 200(2), 463–467. <https://doi.org/10.1016/j.icarus.2008.12.006>
- Knudson, C. A., Perrett, G. M., McAdam, A. C., Campbell, J. L., Flannigan, E. L., Morris, R. V., et al. (2018). Investigation of mineral phase effects caused by sulfur-bearing minerals in a Cumberland Simulant, using laboratory equivalents of SAM, APXS, and CheMin Mars Science Laboratory instruments. In *49th Lunar and Planetary Science Conference, Abstract #2316*. The Woodlands, TX.
- Leshin, L., Mahaffy, P., Webster, C., Cabane, M., Coll, P., Conrad, P., et al. (2013). Volatile, isotope, and organic analysis of martian fines with the Mars Curiosity rover. *Science*, 341(6153), 1238937.
- Lewis, J. M. T., Eigenbrode, J. L., McAdam, A. C., Pavlov, A. A., Li, X., Bower, D. M., et al. (2019). The preservation and detection of lipids in Mars-relevant sulfates and chlorides. In *50th Lunar and Planetary Science Conference, Abstract #2021*. The Woodlands, TX.
- Lewis, J. M. T., Eigenbrode, J. L., Wong, G. M., McAdam, A. C., Archer, P. D., Sutter, B., et al. (2021). Pyrolysis of oxalate, acetate, and perchlorate mixtures and the implications for organic salts on Mars. *Journal of Geophysical Research-Planets*, 126(4), e2020JE006803. <https://doi.org/10.1029/2020JE006803>
- MacKenzie, K. J. D., Berezowski, R. M., & Bowden, M. E. (1986). Thermal and Mossbauer studies of iron-containing hydrous silicates. 6. Minnesotaite. *Thermochimica Acta*, 99, 273–289. [https://doi.org/10.1016/0040-6031\(86\)85290-X](https://doi.org/10.1016/0040-6031(86)85290-X)
- Mahaffy, P. (2013). MSL Mars Sample Analysis at Mars 4 RDR level 1B V1.0 [Dataset]. NASA Planetary Data System. <https://doi.org/10.17189/1519446>
- Mahaffy, P. R., Webster, C. R., Cabane, M., Conrad, P. G., Coll, P., Atreya, S. K., et al. (2012). The Sample Analysis at Mars investigation and instrument suite. *Space Science Reviews*, 170(1–4), 401–478. <https://doi.org/10.1007/s11214-012-9879-z>
- McAdam, A. C., Franz, H. B., Sutter, B., Archer, P. D., Freissinet, C., Eigenbrode, J. L., et al. (2014). Sulfur-bearing phases detected by evolved gas analysis of the Rocknest aeolian deposit, Gale Crater, Mars. *Journal of Geophysical Research-Planets*, 119(2), 373–393. <https://doi.org/10.1002/2013je004518>
- McAdam, A. C., Knudson, C. A., Sutter, B., Franz, H. B., Archer, P. D., Eigenbrode, J. L., et al. (2016). Reactions involving calcium and magnesium sulfates as potential sources of sulfur dioxide during MSL SAM evolved gas analyses. In *47th Lunar and Planetary Science Conference, Abstract #2277*. The Woodlands, Texas.
- McAdam, A. C., Sutter, B., Archer, P. D., Franz, H. B., Wong, G. M., Lewis, J. M. T., et al. (2020). Constraints on the mineralogy and geochemistry of Vera Rubin ridge, Gale crater, Mars, from Mars Science Laboratory Sample Analysis at Mars evolved gas analyses. *Journal of Geophysical Research-Planets*, 125(11), e2019JE006309. <https://doi.org/10.1029/2019JE006309>
- McAdam, A. C., Sutter, B., Franz, H. B., Hogancamp, J. V., Knudson, C. A., Andrejkovicova, S., et al. (2017). Constraints on the mineralogy of Gale crater mudstones from MSL SAM evolved water. In *48th Lunar and Planetary Science Conference, Abstract #1853*. The Woodlands, TX.
- Millan, M., Pozarycki, C., McAdam, A., Andrejkovicova, S., Mahaffy, P. R., Glavin, D., et al. (2020). Optimization of the Sample Analysis at Mars wet chemistry experiment for the detection of organics in Glen Torridon. In *51st Lunar and Planetary Science Conference, Abstract #1897*. The Woodlands, Texas.
- Millan, M., Williams, A. J., McAdam, A. C., Eigenbrode, J. L., Steele, A., Freissinet, C., et al. (2022). Sedimentary organics in Glen Torridon, Gale Crater, Mars: Results from the SAM instrument suite and supporting laboratory analyses. *Journal of Geophysical Research: Planets*, 127, e2021JE007107. <https://doi.org/10.1029/2021JE007107>
- Milliken, R. E., Grotzinger, J. P., & Thomson, B. J. (2010). Paleoclimate of Mars as captured by the stratigraphic record in Gale Crater. *Geophysical Research Letters*, 37, L04201. <https://doi.org/10.1029/2009gl0141870>
- Ming, D. W., Archer, P. D., Glavin, D. P., Eigenbrode, J. L., Franz, H. B., Sutter, B., et al. (2014). Volatile and organic compositions of sedimentary rocks in Yellowknife Bay, Gale crater, Mars. *Science*, 343(6169), 1245267. <https://doi.org/10.1126/science.1245267>
- Mu, J., & Perlmutter, D. D. (1981). Thermal-decomposition of inorganic sulfates and their hydrates. *Industrial and Engineering Chemistry Process Design and Development*, 20(4), 640–646. <https://doi.org/10.1021/i200015a010>
- Navarro-González, R., Navarro, K. F., Coll, P., McKay, C. P., Stern, J. C., Sutter, B., et al. (2019). Abiotic input of fixed nitrogen by bolide impacts to Gale crater during the Hesperian: Insights from the Mars Science Laboratory. *Journal of Geophysical Research-Planets*, 124(1), 94–113. <https://doi.org/10.1029/2018je005852>
- NIST Mass Spectrometry Data Center, & Wallace, W. E. (2019). Mass spectra. In P. J. Linstrom, & W. G. Mallard (Eds.), *NIST Chemistry WebBook, NIST Standard Reference Database Number 69*. National Institute of Standards and Technology.
- O'Connell-Cooper, C. D., Thompson, L. M., Spray, J. G., Berger, J. A., Gellert, R., McCraig, M., et al. (2022). Statistical analysis of APXS-derived chemistry of the clay-bearing Glen Torridon region and Mount Sharp group, Gale crater, Mars. *Journal of Geophysical Research: Planets*, 127, e2021JE007177. <https://doi.org/10.1029/2021JE007177>
- Peretyazhko, T. S., Pan, M. J., Ming, D. W., Rampe, E. B., Morris, R. V., & Agresti, D. G. (2019). Reaction of akaganite with Mars-relevant anions. *ACS Earth and Space Chemistry*, 3(2), 314–323. <https://doi.org/10.1021/acsearthspacechem.8b00173>

- Rampe, E. B., Bristow, T. F., Morris, R. V., Morrison, S. M., Achilles, C. N., Ming, D. W., et al. (2020). Mineralogy of Vera Rubin ridge from the Mars Science Laboratory CheMin instrument. *Journal of Geophysical Research-Planets*, 125(9), e2019JE006306. <https://doi.org/10.1029/2019JE006306>
- Rampe, E. B., Ming, D. W., Blake, D. F., Bristow, T. F., Chipera, S. J., Grotzinger, J. P., et al. (2017). Mineralogy of an ancient lacustrine mudstone succession from the Murray formation, Gale crater, Mars. *Earth and Planetary Science Letters*, 471, 172–185. <https://doi.org/10.1016/j.epsl.2017.04.021>
- Rampe, E. B., Morris, R. V., Archer, P. D., Agresti, D. G., & Ming, D. W. (2016). Recognizing sulfate and phosphate complexes chemisorbed onto nanophase weathering products on Mars using in-situ and remote observations. *American Mineralogist*, 101(3–4), 678–689. <https://doi.org/10.2138/am-2016-5408CCBYNCND>
- Sklute, E. C., Jensen, H. B., Rogers, A. D., & Reeder, R. J. (2015). Morphological, structural, and spectral characteristics of amorphous iron sulfates. *Journal of Geophysical Research-Planets*, 120(4), 809–830. <https://doi.org/10.1002/2014je004784>
- Stern, J. C., Sutter, B., Freissinet, C., Navarro-González, R., McKay, C. P., Archer, P. D., et al. (2015). Evidence for indigenous nitrogen in sedimentary and aeolian deposits from the Curiosity rover investigations at Gale crater, Mars. *Proceedings of the National Academy of Sciences*, 112(14), 4245–4250.
- Sutter, B., McAdam, A. C., Archer, P. D., Ming, D. W., Eigenbrode, J. L., Rampe, E. B., et al. (2020). Geochemical processes along and above the Glen Torridon/Greenheugh Pediment unconformity, Gale crater, Mars: Results from the Sample Analysis at Mars instrument. In *Fall AGU Meeting, Abstract #P070-007, San Francisco, CA*.
- Sutter, B., McAdam, A. C., Mahaffy, P. R., Ming, D. W., Edgett, K. S., Rampe, E. B., et al. (2017). Evolved gas analyses of sedimentary rocks and eolian sediment in Gale Crater, Mars: Results of the Curiosity rover's Sample Analysis at Mars instrument from Yellowknife Bay to the Namib Dune. *Journal of Geophysical Research-Planets*, 122(12), 2574–2609. <https://doi.org/10.1002/2016je005225>
- Thorpe, M. T., Bristow, T. F., Rampe, E. B., Tosca, N. J., Grotzinger, J. P., Bennett, K. A., et al. (2022). Mars Science Laboratory CheMin data from the Glen Torridon region and the significance of lake-groundwater interactions in interpreting mineralogy and sedimentary history. *Journal of Geophysical Research: Planets*, 127, e2021JE007099. <https://doi.org/10.1029/2021JE007099>
- Vaniman, D. T., Bish, D. L., Ming, D. W., Bristow, T. F., Morris, R. V., Blake, D. F., et al. (2014). Mineralogy of a mudstone at Yellowknife Bay, Gale Crater, Mars. *Science*, 343(6169). <https://doi.org/10.1126/science.1243480>
- Wang, Y. J., Lu, S., Ren, T. S., & Li, B. G. (2011). Bound water content of air-dry soils measured by thermal analysis. *Soil Science Society of America Journal*, 75(2), 481–487. <https://doi.org/10.2136/sssaj2010.0065>
- Wattel-Koekkoek, E. J. W., Buurman, P., van der Plicht, J., Wattel, E., & van Breemen, N. (2003). Mean residence time of soil organic matter associated with kaolinite and smectite. *European Journal of Soil Science*, 54(2), 269–278. <https://doi.org/10.1046/j.1365-2389.2003.00512.x>
- Westphal, G., Gerhard, K., Wilhelm, W., Ambatiello, P., Geyer, H., Epron, B., et al. (1997). *Sodium chloride*. In *Ullmann's Encyclopedia of Industrial Chemistry, 5th edition* (Vol. 33, pp. 319–365). Wiley-VCH Publishers.
- Williams, A. J., Eigenbrode, J., Floyd, M., Wilhelm, M. B., O'Reilly, S., Johnson, S. S., et al. (2019). Recovery of fatty acids from mineralogic Mars analogs by TMAH thermochemolysis for the Sample Analysis at Mars wet chemistry experiment on the Curiosity rover. *Astrobiology*, 19(4), 522–546. <https://doi.org/10.1089/ast.2018.1819>
- Williams, A. J., Eigenbrode, J. L., Millan, M., Williams, R. H., Buch, A., Teinturier, S., et al. (2021). Organic molecules detected with the first TMAH wet chemistry experiment, Gale crater, Mars. In *52nd Lunar and Planetary Science Conference, Abstract #1763, Virtual*.
- Wong, G. M., Lewis, J. M. T., Knudson, C. A., Millan, M., McAdam, A. C., Eigenbrode, J. L., et al. (2020). Detection of reduced sulfur on Vera Rubin ridge by quadratic discriminant analysis of volatiles observed during evolved gas analysis. *Journal of Geophysical Research-Planets*, 125(8), e2019JE006304. <https://doi.org/10.1029/2019JE006304>
- Wong, G. M., Franz, H. B., Clark, J. V., McAdam, A. C., Lewis, J. M. T., Millan, M., et al. (2022). Oxidized and reduced sulfur observed by the Sample Analysis at Mars (SAM) instrument suite on the Curiosity rover within the Glen Torridon region at Gale crater, Mars. *Journal of Geophysical Research: Planets*, 127, e2021JE007084. <https://doi.org/10.1029/2021JE007084>

## References From the Supporting Information

- Arutyunov, V. S., Basevich, V. Y., Vedenev, V. I., Sokolov, O. V., Ushakov, V. A., & Chernysheva, A. V. (1991). Kinetics of the reduction of sulfur-dioxide. 3. Formation of hydrogen-sulfide in the reaction of sulfur-dioxide with hydrogen. *Kinetics and Catalysis*, 32(5), 1112–1115.
- Steele, A., McCubbin, F. M., Fries, M., Kater, L., Boctor, N. Z., Fogel, M. L., et al. (2012). A reduced organic carbon component in martian basalts. *Science*, 337(6091), 212–215. <https://doi.org/10.1126/science.1220715>